EMBRITTLEMENT STUDIES IN AUSTENITIC STAINLESS STEELS

RAMACHANDRAN V. CHELAKARA
B.Tech., Indian Institute of Technology, Bombay, 1987

A thesis submitted to the faculty
of the Oregon Graduate Institute
of Science and Technology
in partial fulfillment of the
requirements for the degree
Master of Science
in
Materials Science and Engineering

October, 1993

The thesis "Embrittlement Studies in Austenitic Stainless Steels" by Ramachandran V. Chelakara has been examined and approved by the following Examination Committee:

David G. Atteridge
Associate Professor
Thesis Research Advisor

Jack H. Devletian
Professor

Stephen M. Bruemmer
Adjunct Faculty Member

DEDICATED TO MY PARENTS

TABLE OF CONTENTS

ACKNOWLEDGEMENTS

The author gratefully acknowledges the Department of Energy(DOE) for funding this research work. I wish to thank my research advisor, Dr. David Atteridge for providing me the technical support for this work. His patience and understanding during the course of this researc work is acknowledged. Thanks are also due to Dr. Stephen Bruemmer for providing crucial technical expertise for the project and Dr. Jack Develetian for examining this thesis.

I cannot overlook John Simmons' help in the compilation of this thesis. He and the rest the OGI staff and students did more than their share to make my stay at OGI an enjoyable one. Thanks are extended to Deva, Sudarsan, Partha, Vivek, Chen and Rajesh for their support.

FIGURES

TABLES

NOMENCLATURE

SS	Stainless Steel
IG	Intergranular
CVN	Charpy-V notch
SEM	Scanning Electron Microscope
DOS	Degree of Sensitization
EPR	Electrochemical Potentiokinetic Reactivation
TTP	Time-Temperature-Precipitation
AEM	Auger Electron Spectroscopy
LCHP	Low C-High P
MCLP	Medium C-Low P
SA	Solution Annealed
LN	Liquid Nitrogen
HCHP	High C-High P
HCLP	High C-Low P
HCNP	High C-No P
NCHP	No C-High P
HCMP	High C-Medium P
M_s	Martensite Start Temperature
MCHP	Medium C-High P
OGI	Oregon Graduate Institute

ABSTRACT

Embrittlement Studies in Austenitic Stainless Steels

Ramachandran V. Chelakara, M.S.

Oregon Graduate Institute, 1993

Supervising Professor: David G. Atteridge

Embrittlement in austenitic stainless steels may occur as a result of exposure to temperature between 600°C and 900°C. The primary purpose of this investigation was to study the various causes of embrittlement in 304 and 316 Type stainless steels. The potential causes o embrittlement are

(1) Grain boundary carbide precipitation
(2) Grain boundary phosphorus segregation
(3) Grain boundary martensite formation
(4) Sigma phase formation

In addition, the effect of these embrittling mechanisms on the impact energy was quantified and assessed on the basis of their potency. Heat treatments of solution annealed 304 and 316 stainless steels were performed for different aging times at temperatures between 500°C and 1000°C. The impact energy was measured by the Charpy V-notch impact test. The extent o carbide precipitation was assessed using the Electrochemical Potentiokinetic Reactivation(EPR) test. The amount of phosphorus segregation to grain boundaries was determined by Auger measurements at grain boundaries of fractured surfaces.

The carbide at grain boundaries was found to be the controlling factor in intergranular embrittlement. Phosphorus segregation to grain boundaries is not necessary to induce

intergranular embrittlement. Sigma precipitation from delta-ferrite at short aging times and results in a severe reduction of impact toughness.

INTRODUCTION

Austenitic stainless steels (SS) are often used as structural materials in thermal and nuclear power plants as well as chemical processing plants. They are also used in cryogenic applications because of their low temperature toughness. However, certain heat treatments can promote a dramatic loss in toughness as measured by high strain rate testing, for both 304 and 316 SS at temperatures at and below ambient.[1-10]

Thermal treatments in the temperature range of 500 to 1000°C can induce microstructural and microchemical changes in the material and lead to severe embrittlement problems under impact loading conditions. Embrittlement in these steels has been connected to a variety of mechanisms. Precipitation of $M_{23}C_6$ type chromium-rich carbides at the grain boundaries, which occurs when the material has been exposed to temperatures in the range 600 to 900°C, has been mentioned as promoting embrittlement.[7-11]

A number of recent results have suggested that the segregation of impurity elements like P and S can contribute to intergranular (IG) embrittlement.[3,12,13] In addition, grain boundary martensite formation and sigma phase precipitation have been cited to cause severe reductions in impact toughness.[6-17]

The work reported herein was undertaken to determine the cause of impact-induced low ductility failure in Type 304 and 316 SS. Potential causes of embrittlement in austenitic SSs were studied and their influence on impact properties measured by the Charpy-V-notch (CVN) test. The degree of sensitization (DOS), an indication of chromium depletion at grain boundaries, was measured by the electrochemical potentiokinetic reactivation (EPR) test. Fracture morphologies obtained by impact testing were analyzed by the use of scanning electron microscopy (SEM).

The major objective of this work was to obtain data which would assess the potential embrittlement mechanisms and determine their embrittling potency. The potential causes of embrittlement discussed herein are:

- Grain boundary precipitation of Cr-rich carbides
- Grain boundary segregation of P
- Formation of grain boundary martensite
- Precipitation of sigma phase

BACKGROUND

Austenitic SSs are susceptible to IG embrittlement as measured by impact testing after they have been subjected to temperatures between 600 and 900°C. Impact-induced embrittlement in these steels occurs by various mechanisms. The following discussion reviews the various potential causes of the embrittlement in austenitic SSs, namely:

- The presence of carbides like $M_{23}C_6$ on the grain boundaries
- Segregation of impurities like P to the grain boundaries
- Formation of martensite at grain boundaries
- Precipitation of brittle intermetallic phases like sigma

GRAIN BOUNDARY PHOSPHORUS SEGREGATION

Solute elements with limited bulk solubilities are often found to have significantly higher chemical compositions at surfaces and interfaces (i.e., grain boundaries) in engineering materials. Such preferential enrichment of alloy or impurity solute atoms occurs due to decreasing matrix solute solubility with decreasing temperature and basically unlimited solute solubility at surfaces and interfaces. This latter solubility is due to the structure disorder inherent at surfaces and interfaces, which results in high energy atom configurations which readily accept solute atoms. This phenomenon is called segregation.

The lattice distortion produced by solute atoms may be considerable. If this strain energy can be relieved by segregation to a region that is already distorted, i.e., a grain boundary, it provides a large driving force for such segregation. It is also postulated that impurity atoms can form low energy atomic metallic, ionic, and/or covalent atomic bonding "arrangements" at grain boundaries not possible in the matrix.[18]

Approach to Equilibrium

The most common embrittling impurity element in steels systems is P. Consequently, its segregation to grain boundaries has been studied extensively. The segregation mechanism of P is classified as the "equilibrium" type[19] since the rate of IG buildup increases with temperature while the maximum segregation decreases as temperature is raised.

The kinetics of grain equilibrium boundary segregation, as derived by McLean[20], can be expressed by:

$$\frac{C_{gbt} - C_{gb0}}{C_{gb\infty} - C_{gb0}} = 1 - \exp \frac{4Dt}{\alpha_2^2 d^2} \left[1 - erf \frac{2\sqrt{(Dt)}}{(\alpha_2 d)}\right] \qquad (1)$$

where,

C_{gbt} is the grain boundary concentration after time t.

$C_{gb\infty}$ is the equilibrium grain boundary concentration attained after infinite time.

C_{gbo} is the initial grain boundary concentration.

C_1 is the grain interior concentration, assumed constant.

α is the ratio for $\frac{C_{gb}\alpha}{C_1}$

D is the diffusion coefficient at that temperature.

t is the time.

d is the thickness of the grain boundary.

Grain boundary concentration is calculated to build up relatively quickly to about half its equilibrium value with the rate of build up slowing down as higher concentrations are reached, Figure 1. The time to reach the half-way mark is given by

$$\frac{2\sqrt{(Dt)}}{\alpha_2 d} = \frac{3}{4} \tag{2}$$

or

$$t_{0.5} = \frac{9\alpha_2^2 d^2}{64D} \tag{3}$$

Guttmann et al. approximates Equation (1) by

$$C_{gb}(t) - C_{gb}(0) = 4C_1 \left(\frac{Dt}{\Pi a^2}\right)^{1/2} \tag{4}$$

where a is the average atomic diameter. These expressions can be used to eliminate grain boundary concentrations of P as a function of aging time, temperature and bulk P concentration.

Influence of Other Solutes

A second solute element may affect the rate and degree of segregation by affecting the rate of diffusion, or by displacing or stabilizing the solute atom from at its preferred lattice site. It is postulated that the second solute element tends to displace the first from distorted regions, if the second solute element has a larger misfit of the same sign as the first, which increases the tendency of the first element to segregate. If the two have misfits of opposite signs and are present in about equal atomic proportions, then they tend to 'pair off' in the lattice with the result that the

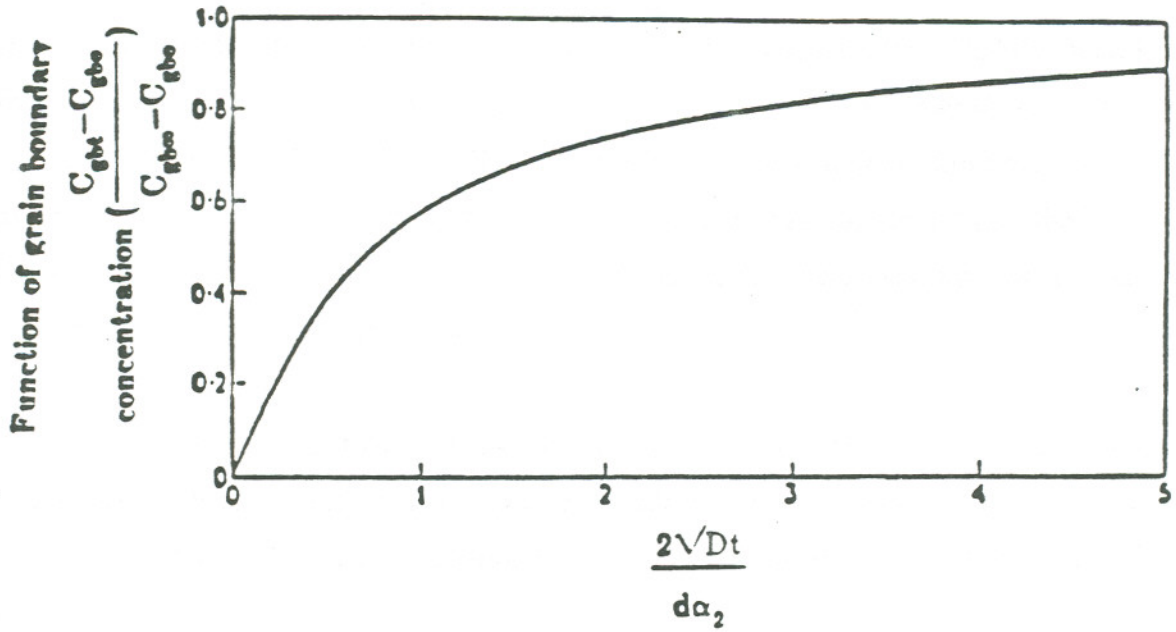

FIGURE 1. Change in Grain Boundary Concentration with Time for Initial Value C_{gbo} to Final Equilibrium Value $C_{gb\infty}$.

tendency to segregate is reduced. Even if the degree of the second element misfit is not high, it may still be high enough to affect the average lattice parameter sufficiently to influence the degree of segregation of the other solute.[18]

These factors become important when considering the influence of different substitutional alloying elements such as Ni, Mn, and Cr and other impurity elements like S on the segregation characteristics of P. Most studies into interaction effects of other solutes have been done on simple ternary systems and are not directly applicable to the highly complicated case of complex alloy steels like 304 and 316 SSs.

Thermodynamics of Segregation

The P concentration at grain boundaries will be controlled by the thermodynamics and the kinetics of P diffusion in the lattice. Therefore, thermal

history is the key factor that determines the extent of P segregation for a "given" bulk P composition/grain size. Phosphorus segregation in 304 and 316 SS is significant in the temperature range of 600 to 850°C. Bulk solubility goes up at higher temperatures reducing the thermodynamic driving force for segregation. On the other hand, the diffusion of P becomes sluggish at lower temperatures, and it becomes difficult to reach the thermodynamic equilibrium level.

Segregation can be thought of as the distribution of the solute between two phases if one treats the grain boundary as one phase and the matrix as another.[18] The distribution of P between phases can then be discussed in terms of equilibrium concentrations given by:

$$P_{mat} \leftrightarrow P_{gb} \qquad (8)$$

where P_{mat} is the P matrix concentration and P_{gb} is the grain boundary phase concentration. The equilibrium constant K_T for this reaction defined as:

$$K_T = \frac{a^P_{gb}}{a^P_{mat}} = \frac{\gamma^P_{gb}\ P_{gb}}{\gamma^P_{mat}\ P_{mat}}$$

where a^P_x is the activity and γ^P_x is the activity coefficient for P in the given phase. This equilibrium constant is simply the enrichment factor first reported by Seah and Hondros[21] which can determined by Auger measurements of grain boundary compositions. The fact that K decreases with increasing temperature is not surprising because, as the temperature is raised, the increased entropy causes desegregation. It is interesting to note that the ratio of concentration decreases with increasing P_{mat} at constant temperatures as the increase in concentration at the grain boundaries does not keep up proportionally with the increase in concentration in the matrix, even though the ratio of activities remains constant. It is postulated that this happens due to repulsion between impurity atoms which increasing concentration or that the segregant must occupy sites that are of increasingly higher energy as the concentration in the boundary is increased.

A second type of segregation to be considered is competitive segregation between two elements in which the presence of one element limits the amount that a second element can segregate. Assuming sulfur is the second element, the equilibrium reaction can be written as:

$$S_{mat} + P_{gb} \leftrightarrow S_{gb} + P_{mat}$$

and

$$K = \frac{a_{gb}^{S}\, a_{mat}^{P}}{a_{mat}^{S}\, a_{gb}^{P}}$$

If, for instance, sulfur is precipitated as a sulfide by the addition of a strong sulfide former a_{mat}^{S} would be lowered, but, in order to keep K constant, a_{gb}^{S} would also need to decrease.[7,22] Third element effects can also be assessed using this type of relationship.

Diffusion Coefficients for Phosphorus

Gruzin et. al.[23] estimated the diffusivity of P in α-Fe to be $D_p = 71.0\exp\left(\frac{-20000}{T}\right)\frac{cm^2}{sec}$. This corresponds to $D_0 = 0.007\frac{cm^2}{sec}$ and Q = 40 kcal/mole. Guttman et. al.,[24] using a modified Mclean equation and an Arrhenius plot of D_p v/s 1/T, estimated the pre-exponential factor and the activation energy to be $D_0 = 20.62\frac{cm^2}{sec}$ and Q = 230KJ/mole in a austenitic Fe-Ni alloy.

The diffusivity of P in Type 304 SS is not known. Briant[25] determined the amount of time needed for equilibrium segregation in Type 304 SS at a variety of temperatures and calculated $\sqrt{Dt}$ values for those temperatures. From this, D_o is estimated to be $D_0 = 20.62\frac{cm^2}{sec}$ and Q = 70 cals/mole. As can be seen, there is a wide disparity

between the values reported for the diffusion coefficients for P in a multi-component system.

As discussed earlier, the addition of an extra element affects the segregation mechanism and thereby influences the diffusivity calculations. For instance, Gruzin and Mural[23] show that Mn increases the diffusivity of P in α-Fe but Mo and Cr retard it. In contrast, most other researchers report that addition of Ni, Mn, and Cr in low-alloy steel will enhance P segregation due to the phenomenon of co-segregation. These effects are generally rationalized by Guttmann's thermodynamic analysis of co-segregation. Calculation of interaction coefficients for different elements with P were made available by Guttman.[19] However, these have been limited to segregation in $\alpha-Fe$ and certain other ternary systems.

Little quantitative information is known about P diffusion/segregation in 304 and 316 austenitic SSs. Briant and Andresen[26] reported a P/Fe peak height ratio of approximately 32% at 600°C and 10% at 700°C for a 304 SS. For 316 SS, they reported a ratio of 6-10% at 600°C and around 10% at 700°C. Both of these measurements were recorded for heats containing a bulk P content of 0.06 wt%. Hanninen and Minni[27] report a maximum P peak to height ratio of 8-10% at 725°C. While for 304 SS, Lumsden[28] reported a maximum of 25 at% after 500 hours of aging at 500°C.

There is substantial evidence that segregation in Type 304 SS occurs to a much greater extent than in Type 316 SS. The major cause for the decreased segregation in Type 316 SS has been postulated to be the presence of the substantial amount of Mo in the alloy. Molybdenum has been considered to have a strong binding energy with P in Fe and it has been postulated that Mo has a direct effect on decreasing P diffusion and segregation by forming Mo-P complexes. Molybdenum has also been seen to indirectly affect P segregation by having a retarding influence on $M_{23}C_6$ carbide precipitation.[29] This

means that there is more free P at the grain boundary which, in turn, leads to a competition for sites with the segregated P at the grain boundary.

Effect of Phosphorus Segregation on Embrittlement

There have been reports in the literature[2,11,13,16] citing the influence of segregated P to the grain boundaries on the development of IG fracture of Type 304 SS. Danyluk et. al.[2,7,11] found that the low temperature impact strength of a high C, P-doped heat of 304 SS show a considerable reduction in impact energy as a function of heat treatment times at temperatures in the carbide precipitation/P segregation range. The authors attributed the embrittlement effect to P segregation without discussion of the influence of other microstructural features on the impact energy.

Explanations of segregation-induced IG fracture have emphasized the effect of impurities on interfacial energy, size effects of impurities at grain boundaries, the energy balance between dislocation nucleation (crack blunting) and IG crack extension, and alteration in chemical bonding across the grain boundary by segregated impurities. Hondros and Mclean[30] proposed that the reduction in the Griffith fracture stress σ_f is due to the alteration of grain boundary surface energy E_γ due to the segregation.

$$\sigma_f = \left(\frac{2E_\gamma}{\Pi c}\right)$$

Where, c is the crack length.

Seah[31] demonstrated that the above analysis was too simple and proposed an atom misfit model to explain the shift in the ductile-brittle transition temperature in α-Fe and argued that large atoms segregated to the grain boundaries increased the interatomic spacing and therefore decreased the IG cohesive stress. He expressed the cohesive stress σ_s as a function of atom size as follows:

$$\sigma_s = \frac{\sigma_o 2a_o}{(a_s + a_o)}$$

where, σ_o is the cohesive stress in the absence of impurities, a_o is the average interatomic spacing across the boundary in the absence of impurities, and a_s is the atomic radius of the impurity. Phosphorus has a reasonably big atomic size and can, therefore, be considered to be embrittling. Bernstein et. al.[32] concluded that the impurities made the grain boundaries more resistant to the passage of dislocations. In this way, impurities may alter the structure of grain boundaries as well as altering their surface energies and chemical bonding.

GRAIN BOUNDARY CARBIDE PRECIPITATION

The precipitation of Cr-rich $M_{23}C_6$ in austenitic SSs is dependent on the free energy of formation, i.e., precipitation will only occur if the reaction is thermodynamically favored. The formation of these carbides require a supersaturation of C in the austenite matrix. Carbide precipitation occurs readily in austenitic SSs due to the low solid solubility of C. The C solubility depends on bulk composition and the temperature of aging amongst other things. Natesan and Kassner[33] describes the solubility of C in Type 304 SS as

$$S_c(wt\%) = 1088 \exp(-23653/RT)$$

Deighton[34] gives the solubility of C in Type 316 SS as

$$S_c(wt\%) = 0.237 \exp(-6272/_T)$$

The above relationships predict that the solubility limit is exceeded in a 0.08% alloy at ~980 and ~1015°C for a 304 and 316 SS alloy, respectively, while in a 0.02wt% alloy the limits are ~820 and ~870°C. The C solubility of 316 SS varies with temperature as shown in Figure 2.

As mentioned earlier, precipitation of the carbide is a function of thermal treatment and bulk composition (primarily C) of the heat. A typical way of illustrating the precipitation behavior is by a time-temperature-precipitation (TTP) diagram. Figure 3 shows the TTP curves[35] for $M_{23}C_6$ precipitation in a 0.038% C, Type 304 SS. This figure indicates the time-temperature domain for the first precipitate of given phase to take place. As indicated in the figure, carbide nucleation and growth occurs first at the interface between delta-ferrite and austenite, followed by
precipitation at austenite grain boundaries, incoherent twin boundaries and finally, at coherent twins.

Other second-phase reactions include precipitation of sigma, chi and laves intermetallics in low C austenitic SSs. Lai[36] discusses the precipitation characteristics of these phases and a TTP diagram of the precipitation sequences for Type 316 SS is shown in Figure 4.

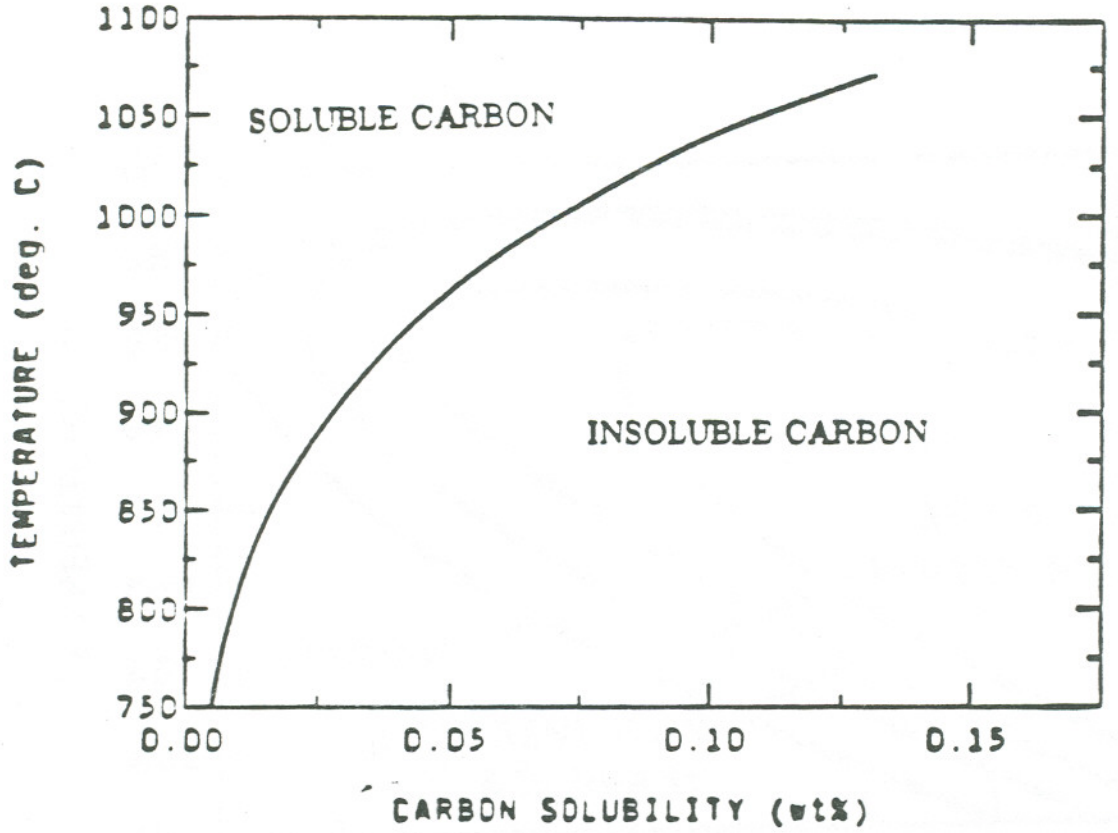

FIGURE 2. Variation of Carbon Solubility with Temperature for 316 SS.[34]

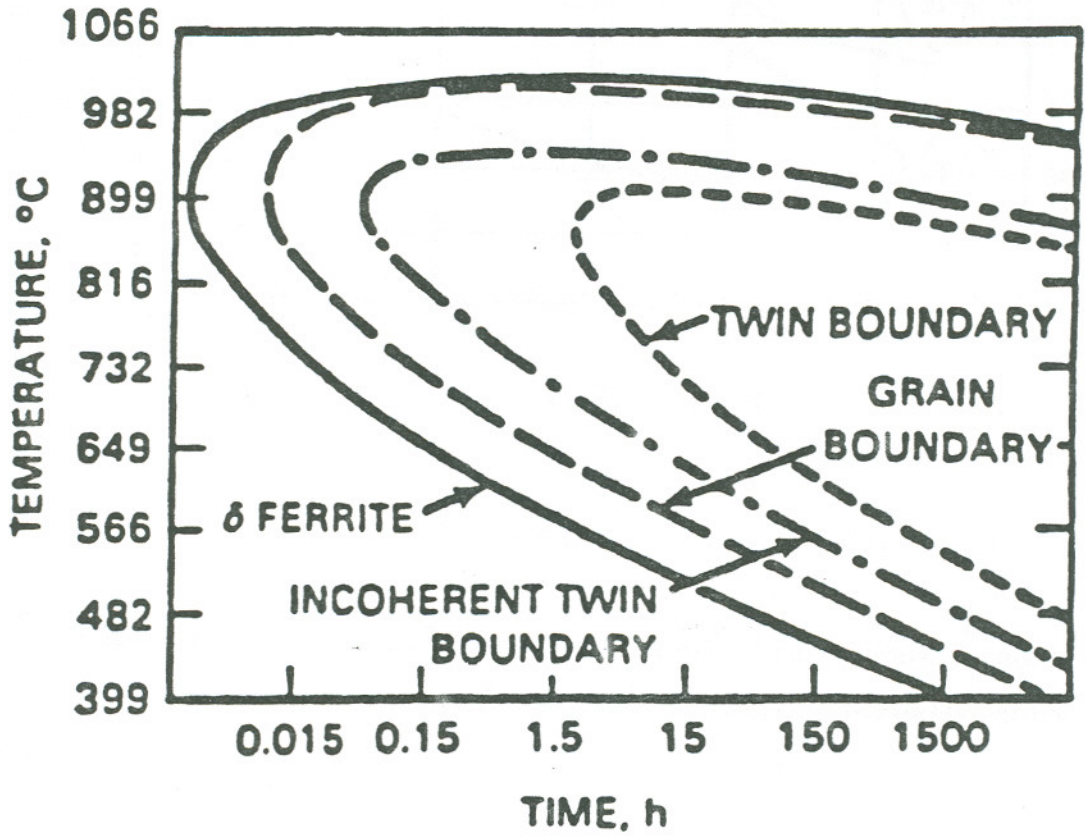

FIGURE 3. Time-Temperature-Precipitation Curves for $M_{23}C_6$ in 0.038 wt% Carbon Type 304 SS.[35]

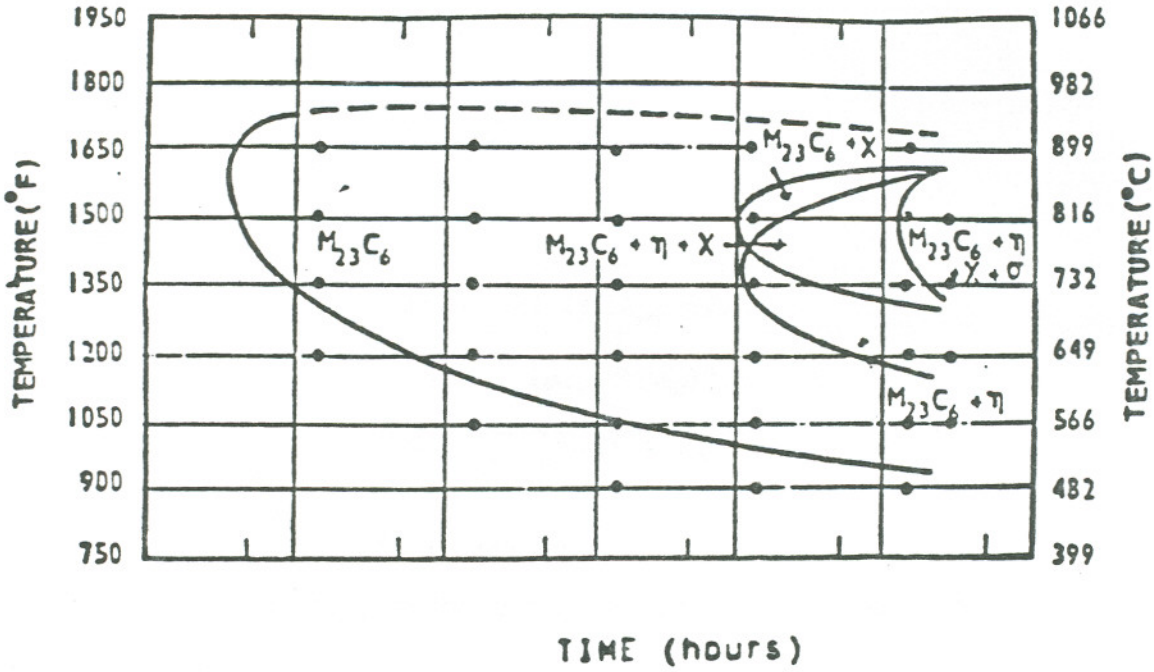

FIGURE 4. Time-Temperature-Precipitation Diagram for Type 316 SS.[35]

The following sections discuss the thermodynamics of carbide precipitation, its effect on IG embrittlement in austenitic SSs and different ways of measuring carbide precipitation.

Thermodynamics of Carbide Precipitation

Stawstrom and Hillert,[37] Tedom et. al.,[38] Hall et. al.,[39] and Fullman[40] have developed several thermodynamic models of carbide precipitation in 300 series austenitic steels to determine the minimum Cr concentration in equilibrium with the carbide at the carbide-matrix interface. The equilibrium reaction between the carbide and the matrix is given below:

$$6C + 23Cr \leftrightarrow Cr_{23}C_6$$

where,

$$\Delta G = -RT \ln(K_{eq}) \text{ and}$$

$$K_{eq} = \frac{1}{(a_{Cr})^{23}(a_C)^6}$$

$$K_{eq} = \frac{1}{(\gamma_{Cr}[Cr])^{23}(a_C)^6}$$

K_{eq} is the equilibrium constant for the reaction, a_c and a_{Cr} are the activities of C and Cr in equilibrium with the carbide, γ_{Cr} is the activity coefficient of Cr in the matrix, and [Cr] is the Cr concentration.

Two of the assumptions made in the development of the thermodynamic model are that the activity of $Cr_{23}C_6$ is assumed to be unity in the above reaction, and that the $M_{23}C_6$ precipitate is $Cr_{23}C_6$. Actually the composition of low temperature carbides from a Type 316 SS have been reported to be $Cr_{16}Fe_5Mo_2C_6$ and to be $Cr_{16}Fe_7C_6$ in Type 304 SS, with both compositions changing as a function of temperature. It was also assumed that the diffusivity of C is so high, compared to that of Cr, that the C activity can be considered constant from the carbide-matrix interface out into the matrix and that C is not depleted below its bulk value.

Effect of Carbide Precipitation on Embrittlement

Several authors in recent years have reported the effect of grain boundary carbide precipitation in austenitic SSs on low-temperature impact and tensile properties in Type 316 SSs. Grain boundary carbides have little effect on the yield and tensile strengths,[5,6,41] they, however, reduce low cycle fatigue properties. A moderate reduction in tensile ductility and a severe reduction in impact energy were found to be caused by densely distributed grain boundary carbides. Fine, dense grain boundary carbides were most detrimental to the low temperature impact energy. However, previous work did not assess

possible segregation effects. Thus, the question remains as to whether carbides were the dominant factor in embrittlement.

The intercrystalline grain boundary cohesive of metal alloys can also be substantially lowered by the presence of a second phase at the grain boundaries. Carbides also promote a local stress concentration at the particle-matrix interface which is postulated to result in subsequent decohesion. High strain rate conditions, such as in a Charpy-V-notch test, would be expected to accentuate the tendency for carbide-induced IG embrittlement. However, not many models have been proposed to quantitatively explain the effect of the precipitate-matrix interface on the susceptibility to IG fracture.

Indirect Method for Measurement of Carbide Precipitation

An indication of the extent of carbide precipitation can be obtained by measuring the DOS of the material. The term 'sensitization' refers to the formation of a Cr depleted region near the grain boundaries which makes the material susceptible to IG corrosion. This depletion results from carbide precipitation, therefore, as the DOS increases, so does the carbide precipitation.

There are several test methods used for determining the extent of carbide precipitation. The test methods range from the ASTM Recommended practices[42] for detecting susceptibility to IG attach in SSs to an EPR technique. The EPR test technique was used in this work and is discussed below.

Electrochemical Potentiokinetic Reactivation Test

The EPR test was used to measure DOS which, in turn, was used as an indicator of the degree of $M_{23}C_6$ carbide precipitation at the grain boundaries. However, a one-to-one relationship between DOS and carbide precipitation is only accurate until the onset of desensitization, i.e., until the Cr level starts building up at the grain boundaries. After this

there is no direct relationship between DOS and further carbide precipitation. In general, the C level in the bulk matrix is substantially depleted by the time desensitization sets in that no further growth of existing precipitates takes place. Microstructural examination of the EPR specimen needs to be undertaken to ascertain that attack is limited to grain boundaries and does not also occur on twins, shearbands, dislocation, etc, if DOS is to be correlated with IG carbide precipitation.

The single loop EPR test was used in this study and consists of developing potentiokinetic curves of a specimen by scanning potentials from the passive to the active region. A passive film is first formed on the surface and the specimen is then scanned through the passive-active (reactivation scan) regimes.[43] This leads to localized film breakdown and attack of regions sufficiently depleted in Cr. If the material is nonsensitized, the passive film will stay intact and suppress the large active peak observed for sensitized SSs. Quantitative measurement of DOS are based on the charge transfer accumulated during the reactivation scan. A schematic of the EPR test scan[44] is shown in Figure 5. The electrolyte used in the EPR test is an aqueous solution of 0.5 M H_2SO_4 + 0.01 M KSCN. Potassium thiocyanate acts as a grain boundary activator and enhances grain boundary attack of a sensitized specimen during the reactivation scan.

The EPR test is a rapid and nondestructive method of (indirectly) indicating the extent of carbide precipitation, at least until the Cr level starts increasing at the grain boundaries. It can discriminate between DOS values for various heats within the same grade for Type 304 and Type 316 SSs[45] and offers a simple and discerning way of comparing propensity for DOS development between SSs of different grades and different grain sizes.

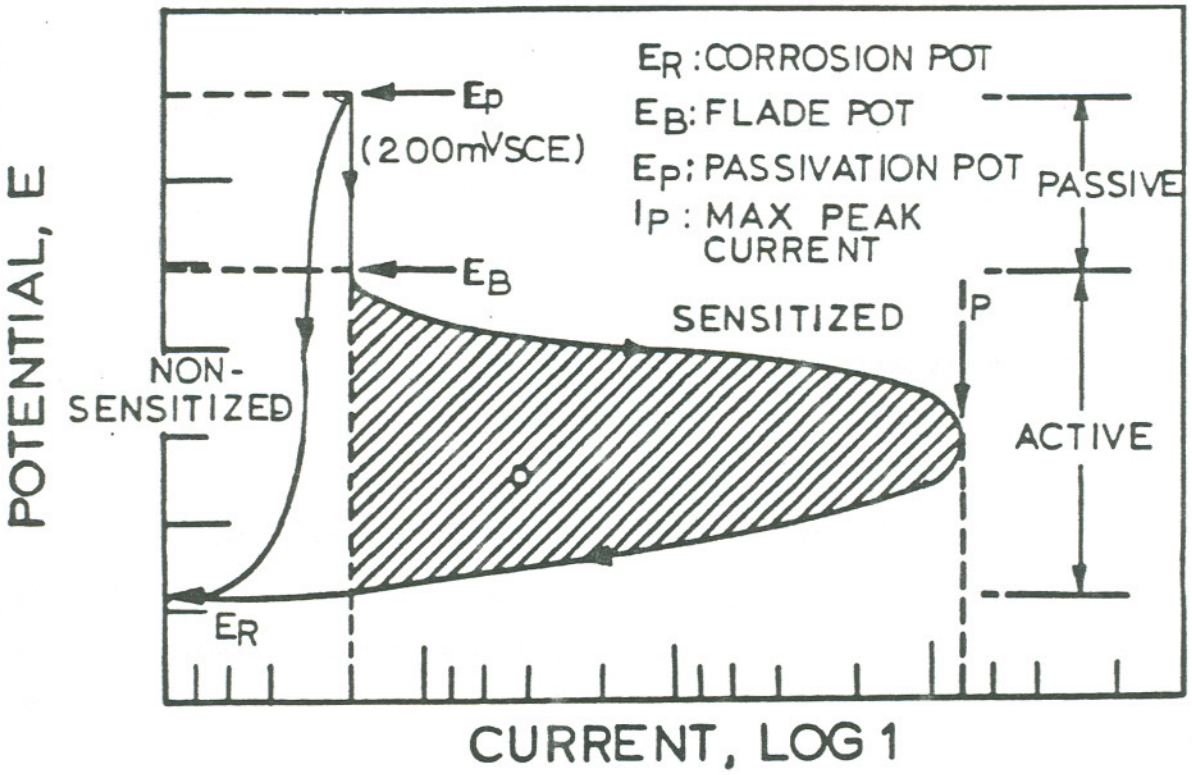

FIGURE 5. Schematic of EPR Test Scan.[33]

GRAIN BOUNDARY MARTENSITIC FORMATION

The precipitation of Cr-rich $M_{23}C_6$ carbides and the subsequent formation of a Cr-depleted zone adjacent to grain boundaries was first explained by Bain and his co-workers.[46] The interstitial C atoms diffuse to the boundaries very rapidly and the subsequent precipitation depletes the matrix and grain boundary regions surrounding the carbide of Cr, which diffuses much more slowly. The Cr and C diffusivity equations for Type 304 and 316 SSs are given below:[35]

For Type 304

$$D_{Cr}=0.08\ \exp(-58500/RT)$$
$$D_{C}=6.18\ \exp(-22450/RT)$$

For Type 316

$$D_{Cr}=6.18 \exp(-63900/RT)$$
$$D_{C}=0.19 \exp(-18820/RT)$$

Since then, several investigators have experimentally confirmed the existence of a Cr-depleted zone adjacent to the precipitated carbides.

Stawstrom, Hillert and Tedmon et. al.[37,38] have derived a theoretical model for predicting the Cr-depleted zone based on the thermodynamics of precipitation and Cr-diffusion kinetics. The width w of the Cr-depleted zone can be estimated by the equation

$$w=2\,[2D_{Cr}\,t]^{1/2}$$

Bulk compositional relations, such as given by Eichelman and Hull,[47] suggest that depletion of elements like Cr and C could raise the M_s temperature and increase the chances for martensite formation at the grain boundaries. Thus, there is a possibility of forming martensite at the grain boundaries, which, in turn, could lead to IG embrittlement.

THE SIGMA PHASE

The sigma phase appears to be the most investigated intermetallic phase in stainless and high alloy steels. The published data on crystal structure, composition, occurrence in various transition metal alloy systems, and effects on physical and mechanical properties have been reviewed by Hall and Algie.[48] Sigma has been reported as an intermetallic phase of electron-compound type with tetragonal crystal structure (c/a = 0.52, 30 atoms per unit cell).

The concept of an 'equivalent Cr parameter' in gauging sigma phase formation is fairly well accepted. To induce sigma formation, the effective equivalent Cr content

should not be less than a critical value (usually from 18 to 25%). The value of this parameter depends on the relative amount of Cr and other ferrite-stabilizing elements which promote sigma precipitation. Nucleation of sigma in austenite requires high-energy interfaces, such as high-angle grain boundaries, incoherent twin boundaries, or high-energy interfaces of second phases, such as oxide inclusions. The occurrence of sigma phase in several common AISI grade SSs like 304, 310, and 316 SS has been reported frequently, and different hypotheses have been brought forward to explain the formation of sigma phase. It forms in both Types 316 and 304 SS as long as the equivalent Cr parameter is high enough to induce sigma phase formation.

Certain authors[49] hold that the σ-phase precipitates via the ferrite formed by the γ-α transformation. In this hypothesis the sigma phase is formed in two stages: in the first, carbides are precipitated and the γ-α transition takes place, while in the second, the σ-phase nucleates, forming at the expense of ferrite. It is postulated that an intermediate σ′ phase forms, having a smaller Cr content than the equilibrium σ-phase. Other authors think differently[49,50] and have found experimentally that σ-phase precipitates directly from austenite. They report that $M_{23}C_6$ carbides precipitate before the σ-phase nucleates.

If, however, the austenitic SSs contain a residual amount of delta-ferrite, the transformation rate of sigma phase is about 100 times faster than the precipitation sequence from gamma to sigma.[50] Here, the sigma phase precipitation occurs mainly through the eutectoid decomposition of delta-ferrite into sigma and gamma. The σ particles nucleate at the δ/γ phase boundaries and grow into the ferrite stringers as γ-σ eutectoid structures. The higher chromium equivalent content in the σ-phase and the almost 100 times greater rate of diffusion of alloying elements in this phase than the austenite renders it susceptible to the formation of σ-phase.

Effect of Sigma Phase on Embrittlement

The most sensitive mechanical test for the presence of σ phase in an alloy is the impact test. Sigma is a highly brittle phase and even the presence of about 1% can seriously affect impact properties. Quite commonly, the effect of sigma on other mechanical properties is not so marked. Hall and Algie[48] showed that a σ-bearing austenitic steel underwent no decrease in tensile strength and only a small change in elongation. The distribution and size of σ particles as well as their fineness is also important to strength and ductility. The effects on corrosion resistance are not as yet well known; however, fine dispersion of the phase along grain boundaries do markedly reduce the resistance to attack by nitric and sulfuric acid, in particular.

Holt and Nicholson[51] have found that sigma precipitated very rapidly from retained delta-ferrite and that the strain induced in the lattice produces high strain energies at the ferrite/austenite grain boundaries which would be expected to lead to conditions favorable to IGSCC. Newell[52] described the precipitation phenomenon as being related first to an initial lattice change or distortion in the ferrite matrix subsequently leading to gross precipitation of the sigma phase. The high strain rate fracture path is reported to follow the original ferrite-austenite matrix interface which has become embrittled by the sigma.

EXPERIMENTAL

This chapter focuses on the experimental procedures adopted and measurement techniques employed in obtaining the results reported in the next chapter. It includes furnace calibration, Charpy impact tests, optical microscopy, EPR test, scanning electron microscopy (SEM) and auger electron spectroscopy. The matrices used for the various experimental methods are also reported.

INITIAL MATERIAL CHARACTERIZATION

Three laboratory heats of Type 304 and four laboratory heats of Type 316 SS were used in this study, Table 1. The compositions of the various heats emphasize the range of C and P compositions. Depending on the C compositions, the heats were labelled as low C, medium C, or high C heats. The P content of the heat was also taken into account. For instance, a low C-high P (LCHP) heat implies a low C, high P heat, medium C-low P (MCLP) implies a medium C low P heat. The particular chemistries have been chosen to isolate carbide precipitation and P segregation effects. The laboratory heats were received in the form of plates with thicknesses of ¼ inch. The plates were in the as-rolled conditions. The heats were vacuum induction melted and then the cast billet was reduced from four inches in thickness to 0.25 inch through a combination of hot forging and hot rolling.

HEAT TREATMENTS

Solution annealing treatments were done in a Lucifer Model - Electrical Muffle Furnace typically at a temperature of 1100°C for 1 hour followed by water quenching. The deformed grains of the as-rolled material recrystallized during this heat treatment, and approached an equilibrium, equiaxed and homogeneous microstructure. This

TABLE 1. Bulk Composition of Laboratory 304 and 316 Type SS Heats

Composition of Laboratory Heats

Heat Number	Remarks	Type	C	Cr	Ni	P	Mn	Mo	Si	Cu	S
1	LCHP	304SS	0.011	20.26	13.92	0.075	1.611	0.017	0.767	0.027	0.011
2	MCLP	304SS	0.042	19.93	13.67	0.005	1.627	0.017	0.67	0.027	0.012
3	HCHP	304SS	0.063	20.26	13.79	0.096	1.716	0.016	0.714	0.026	0.012
4	HCHP	316SS	0.06	16.6	12.05	0.061	1.94	2.0	0.68	-	0.011
5	HCLP	316SS	0.058	17.21	11.31	0.014	1.81	2.28	0.41	-	0.011
6	HCNP	316SS	0.06	17.26	11.86	0.005	1.65	1.94	0.58	-	0.013
7	NCHP	316SS	0.002	15.96	13.24	0.067	1.56	1.96	0.55	-	0.013

chosen solution annealing temperature was much higher than that for complete C solubility for all chemistries used in the study. The 316 SS heats exhibited grain sizes between 120 to 180 μm as a result of this annealing treatment. The 304 SS alloys were subjected to a variety of solution annealing treatments and the grain sizes of the various heats after the respective treatments are listed in Table 2. After the solution annealing treatment, these heats were subjected to a variety of isothermal aging treatments ranging in temperature from 500 to 900°C and up to 100 hours.

TABLE 2. Solution Annealing Treatments and Grain Sizes for 304 Laboratory Heats

Heat Number	Type	SA Treatment hr/1100°C	ASTM No.
3	HCHP	1	140 μm (2.7)
2	MCLP	2	168 μm (2.2)
1	LCHP	1	90 μm (4.0)
1	LCHP	6	145 μm (2.6)
1	LCHP	12	190 μm (1.8)

Furnace Calibration

All the heat treatments were carried out in a Lucifer Model-Electrical Muffle Furnace. The specimens were kept on a 3-inch thick refractory brick at the center of the hot zone. The hot zone was determined by taking temperature profiles along the length of the furnace for a number of temperatures in the range 650 to 1100°C. This was adequate to maintain 2¼-inch long specimens within ± 2°C. The furnace temperature was selected by directly measuring the specimen temperature, which in turn was accomplished by keeping a K-type thermocouple directly above the specimen. Once the target temperature

was chosen, the temperature controller unit of the furnace maintained the hot zone temperature within ± 3°C of it. This means that any part of the heat treated material experienced a temperature within ± 5°C of the reported values.

GRAIN SIZE MEASUREMENT

The average grain size numbers were determined for all heats under study in the solution annealed (SA) condition. The three circle intercept method was used following the guidelines in ASTM Standard E 112-85.[53] Intersection counts were taken on five arbitrarily selected fields of view on each optically prepared specimen. A Zeiss Model optical microscope was used in this study. The working magnification was chosen such that the number of intersections exceeded 70, the specified minimum in ASTM E 112-85, for healthy statistics.

Small test pieces (1 × 1cm) were mounted for optical specimen preparation, ground and metallographically polished, finishing with 0.05 μm alumina powder. They were subsequently electropolished using 60% (by volume) nitric acid electrolyte, with an imposed dc voltage of 1.2 volts. Typically, etching for 100 to 120 seconds produced satisfactory microstructures.

IMPACT TOUGHNESS

The impact toughness of aged specimens was measured using a Tinius Olsen Model Instrumented Charpy Impact Testing machine, following the procedures in ASTM E 23-38.[54] Reduced half thickness standard subsize (Type A) Charpy specimens (55 × 10 × 5mm) were machined from the heat treated slabs. All the specimens were notched in a direction perpendicular to the rolling direction. The fracture toughness was directly noted from the dial of the Tinius Olsen machine. Before starting any series of experiments, the pendulum was given a free swing, to assure this produced zero dial energy, as required. There were three sets of Charpy specimens. The first set was broken at room

temperature, which nominally varied from 19 to 20°C for the entire data set. The second set of Charpy specimens was cooled down to liquid nitrogen temperature (-196°C), equilibrated for half an hour and broken at the Charpy machine within 5 seconds of withdrawal from the liquid nitrogen bath. The third set was equilibrated first at the liquid nitrogen temperature, warmed up to room temperature and equilibrated there for 1 to 2 hours prior to testing.

All the Charpy specimens were cut with their length running along the rolling direction and notched in a direction perpendicular to the rolling direction. The specimen geometry is presented in Figure 6. The specimen for the EPR testing (1 × 1cm) was cut from the edge of the broken Charpy specimen so as to avoid any presence of deformation in the specimen.

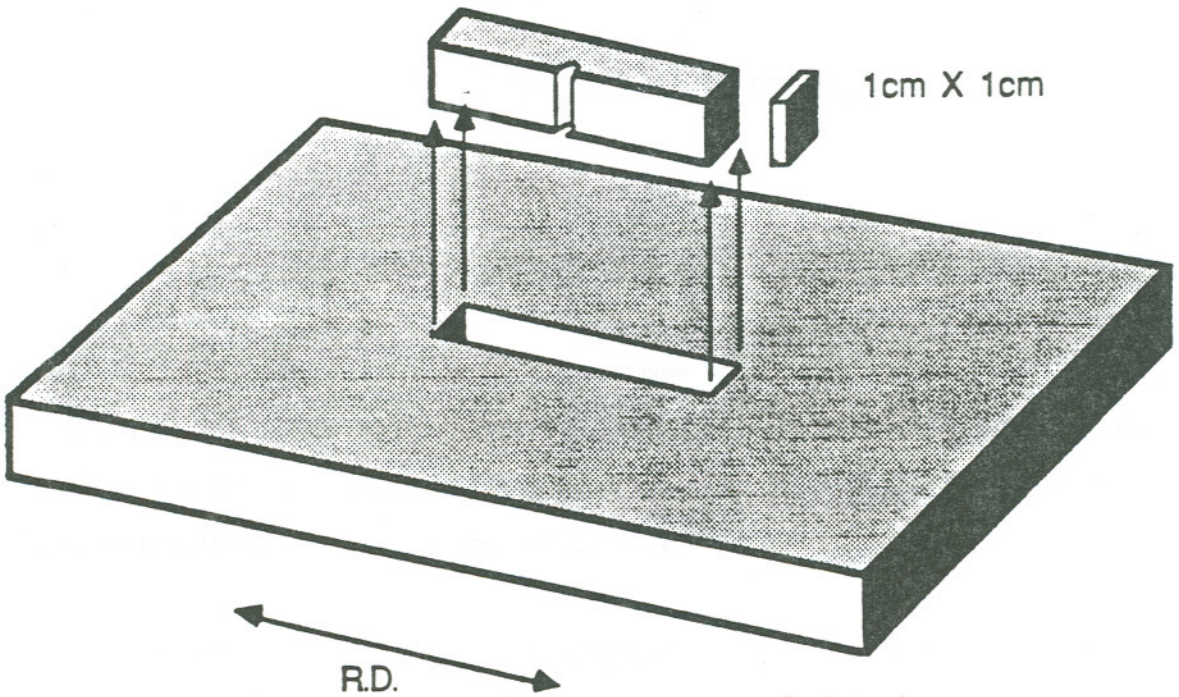

FIGURE 6. Schematic of Specimen Geometry and Orientation for the Charpy Impact Test and Analysis Specimen Optical Metallographic.

QUANTITATIVE FRACTOGRAPHY

The fracture surfaces of the broken Charpy specimens were observed using the JEOL Model JSM 35 scanning electron microscope. A 7 by 7 line grid of size 3½ × 4½ inches was employed to quantify the fracture. This size corresponded to the size of the fracture photographs taken on the SEM. The %age IG fracture was calculated by noting the fraction of test points falling on IG faces and using the following relation:

$$\%I.G.Fracture = \frac{N_{I.G.}}{N_I} X100$$

hence,

$$\%I.G.Fracture = \frac{N_{I.G.}}{81} X100$$

thus,

$$\%I.G.Fracture = 1.234 X N_{I.G.}$$

where,
$N_{I.G.}$ = Number of test points falling on I.G. face
N_T = Total Number of tests points = 81.

Each reported IG fracture was an average of four measured values, measured on four different fields of view at 200X. The fields of view were selected close to the notch and at the central section of the fracture surface. The location of the field of view may lead to differences in the measured values of IG fracture.

MEASUREMENT OF DOS BY EPR TESTING

The degree of sensitization of each test specimen cut from the edge of the broken Charpy bar was measured using the EPR test and is reported as the integrated charge which is normalized to the grain size, Pa, or equivalent DOS value of C/cm^2. The

equipment used for the EPR test was an Instruspec Model WC-5 metal sensitization detector which contains an automated scanning potentiostat and current measuring and integration instruments.

The electrochemical corrosion cell consisted of a specimen holder (the working electrode), an auxiliary electrode (graphite) and a reference electrode (standard calomel electrode). A SS screw was attached to the back of the specimen for an electrical connection. The specimens were then mounted in an epoxy resin and metallographically prepared using standard practices and silicon-carbide abrasive papers of 120 through 600 grit. The final polishing was done with 6 and 1 μm diamond pastes on nylon cloths. A mask with circular area 0.3 cm^2 was used to outline the region of attack in the EPR test. The test parameters are shown in Table 3. A schematic of the test set-up is shown in Figure 7.[35]

TABLE 3. EPR Testing Parameters

Sample Surface Finish	:	1 μm Diamond
Electrolyte	:	0.5M H_2SO_4 = 0.10M KSCN
Electrolyte Temp.	:	30°C ± 1°C
Corrosion Potential (E_c)	:	-0.360 to -0.400 volts (For 304SS)
Passivation Potential (E_p)	:	+ 0.200 volts
Reactivation Scan Rate	:	6 volts/hour (for 304SS)
Instrument	:	Intruspec Model WC-5 Metal Sensitization Detector

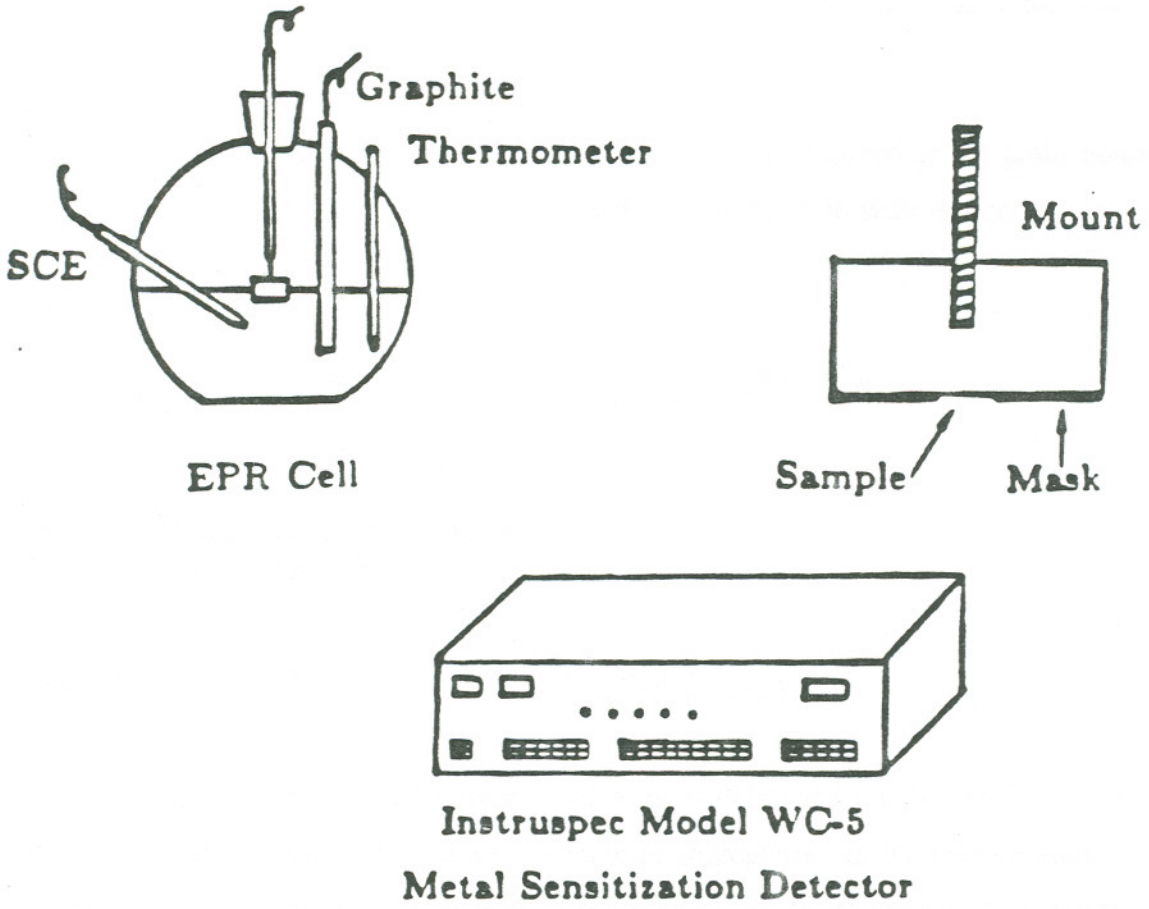

FIGURE 7. Schematic of EPR Test Set-up.[35]

The test cell is set up after the specimen is inserted in the holder and, once the electrolyte has reached the proper temperature, the test is ready to begin. The test can be broken into the following steps:

- The open-circuit corrosion potential, E_c, of the working electrode (compared to the reference electrode) is measured;
- The sample is passivated at a passivating potential, E^p, of + 200 mV;
- The sample is then reactivated by varying the potential through the active region at a constant scan rate (6 volts/hour for 304 SS and 3 volts/hour for 316 SS);

- The area of the reactivation peak is then integrated to give the total charge value, Q.

As mentioned above, this charge value is then normalized to the grain boundary area of each test specimen which is obtained by a correlation with the grain size outlined by Clarke et. al:

$$Pa\ (C/cm^2) = \frac{Q}{A_s\ [5.1x10^{-3}\exp\ (0.35X)]}$$

where,
A_s = Masked specimen area, cm^2
X = ASTM grain size

GRAIN BOUNDARY PHOSPHORUS MONOLAYER COVERAGE

Auger Electron Spectroscopy is the most widely used reliable analytical tool to quantify grain boundary monolayer coverage of segregants. In the present study, P segregation was quantified on selected specimens at Pacific Northwest Laboratory in Richland, Washington, by L. A. Charlot using a high resolution PHI Model 660 Scanning Auger Microscope. Small cylindrical specimens, as per the standard design, were machined out from the fractured Charpy specimens. These were fractured in-situ on the Auger fracture stage at Liquid Nitrogen (LN) temperature (-196°C) and under ultra-high vacuum, background pressure being less than $7X10^{-10}$ torr. The specimens produced satisfactory IG fracture, without any need for hydrogen charging, the latter being the usual way to induce IG fracture for specimens not intrinsically prone to it. Area scans were taken using a primary beam voltage of 5 or 10 KV and probe current either 0.2 or 0.16 μA. The energy resolution was set at 0.6%.

Grain boundary compositions were calculated assuming a sub-monolayer segregation, following the model published by Hondros and Seah.[30] The grain boundary concentration C_i, of an element i, was calculated by:

$$C_i + \lambda \frac{S_{Fe}}{S_i} \frac{I_i}{I_{Fe}} = Q_i \frac{I_i}{I_{Fe}}$$

where, λ is the escape depth of the Auger electrons (which is a function of the incident energy of the Auger electron), S_i and S_{Fe} are the relative sensitivity factors for the element i and the base metal Fe respectively, I_i and I_{Fe} are the peak-to-peak heights of the transitions being measured and Q_i is the conversion ratio. The relative sensitivity factors were obtained from the PHI handbook and are applicable for cylindrical mirror analyzer apparatuses with an energy resolution of 0.6%.

RESULTS AND DISCUSSION

This section presents and discusses research designed to quantify microstructural and microchemical effects on the relative susceptibility of Type 304 and 316 SSs to embrittlement as a function of thermal history. The major embrittlement mechanisms addressed are as follows:

- Grain boundary carbide precipitation
- Grain boundary P segregation
- Grain boundary martensitic formation
- Sigma phase

Embrittlement mechanisms are discussed and then ranked in order of potency in causing low impact energy failure.

The embrittlement studies on Type 316 SS will be discussed initially; the embrittlement studies on the 304 SS will be presented next, followed by a generic discussion of the two materials and significance of the test results.

EMBRITTLEMENT MECHANISMS IN TYPE 316 STAINLESS STEEL

Four 316 SS heats were evaluated. All heats had essentially the same base chemistry except for the C and P content, as listed in Table 2. The four heats consisted of High C-High P (HCHP), High C-Low P (HCLP), High C-No P (HCNP) and No C-High P (NCHP). The following potentially harmful IG embrittlement mechanisms are discussed in the subsections below:

- grain boundary carbide precipitation
- grain boundary P segregation and formation of martensite at Cr-depleted grain boundaries

A subsequent sub-section discusses their interactive effects and their relative embrittlement effect ranking. The data presented in each subsection is aimed at isolation and evaluation

of the individual effects of the various (potential) embrittlement phenomena in order to allow ranking of these effects in their order of potency in causing low impact energy failure.

Effect of Grain Boundary Phosphorus Segregation

This section discusses the influence of P segregation to the grain boundaries on the development of IG fracture in 316 SS. Figures 8 and 9 show the variation in LN temperature impact energy with aging time at 750°C for the NCHP, HCHP, High C-Medium P (HCMP) and HCLP heats. As can be seen, the total impact drop was very small in the NCHP heat in which the only embrittlement mechanism under consideration was P segregation, even at long aging times. The fracture morphologies remained essentially transgranular, Figure 9, thus the drop, however slight, could not be correlated with any particular embrittlement mechanism.

All high C heats, regardless of P content, exhibited substantial drop in impact energy as a function of aging time, Figure 8, and exhibited IG fracture, Figure 9, thus, precipitation of grain boundary carbides, not P, appears to control IG embrittlement. In fact, the High C-"No" P results indicate P is not needed to produce LN embrittlement in 316 SS. It does appear, however, that the presence of P may accentuate IG embrittlement. This is suggested by the observed decrease in impact energy and increase in % IG fractures for the high C heats as a function of increasing P, Figures 8 and 9. The amount of P found by Auger Analysis in grain boundaries in these high C heats as a function of measured P content is given in Table 4, a typical AES analysis is illustrated in Figure 10.

Note that these values are lower than expected, based on previous P measurements by

FIGURE 8. Reduction in Impact Energy as a Function of Heat Treatment Time at 750°C for 316 SS (all heats).

Briant[26] and Lumsden.[28] Thus, it is concluded that segregation, of the amount observed in the heats under consideration, plays a secondary role in promoting IG failure under high strain rate conditions.

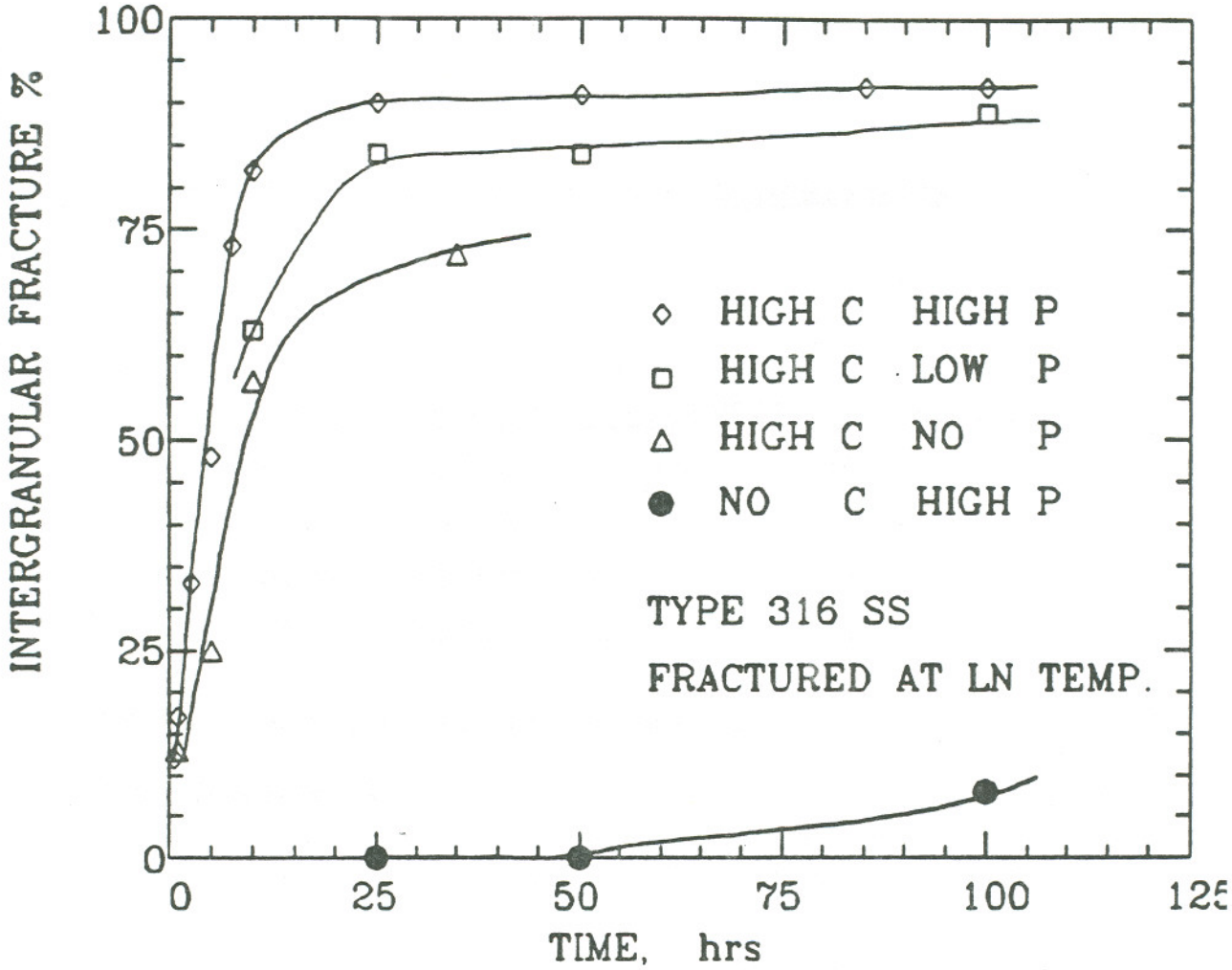

FIGURE 9. Intergranular Embrittlement as a function of Heat Treatment Time at 750°C for 316 SS (all heats).

TABLE 4. Grain Boundary Phosphorus Segregation in 316 Laboratory Heats

Heat Number	Type	Heat Treatment	P/Fe PHR,*%	%Monolayers
1	HCLP	Step Cool	0-5, 1.8	0-3, 1.0
2	HCHP	800C/100hr	5-10, 7.2	4-7, 5.4
3	HCHP	750C/100hr	N.A.	8
4	HCHP	Step Cool	N.A.	10

* Range and Average of Measured Levels are Listed

PHR = Peak Height Ratio

A stepped heat treatment was carried out on the HCHP heat, in an attempt to maximize segregation to the grain boundaries. The stepped treatment started at 800°C for 10 hours and ended at 650°C for 100 hours. The amount of segregated P at the grain boundaries, obtained by an Auger analysis, was approximately 10% in comparison to 8% P after 100 hours at 780°C for the same heat. The fracture morphologies for the stepped treatment is presented in Figure 11. Fracture follows the carbide-matrix interface.

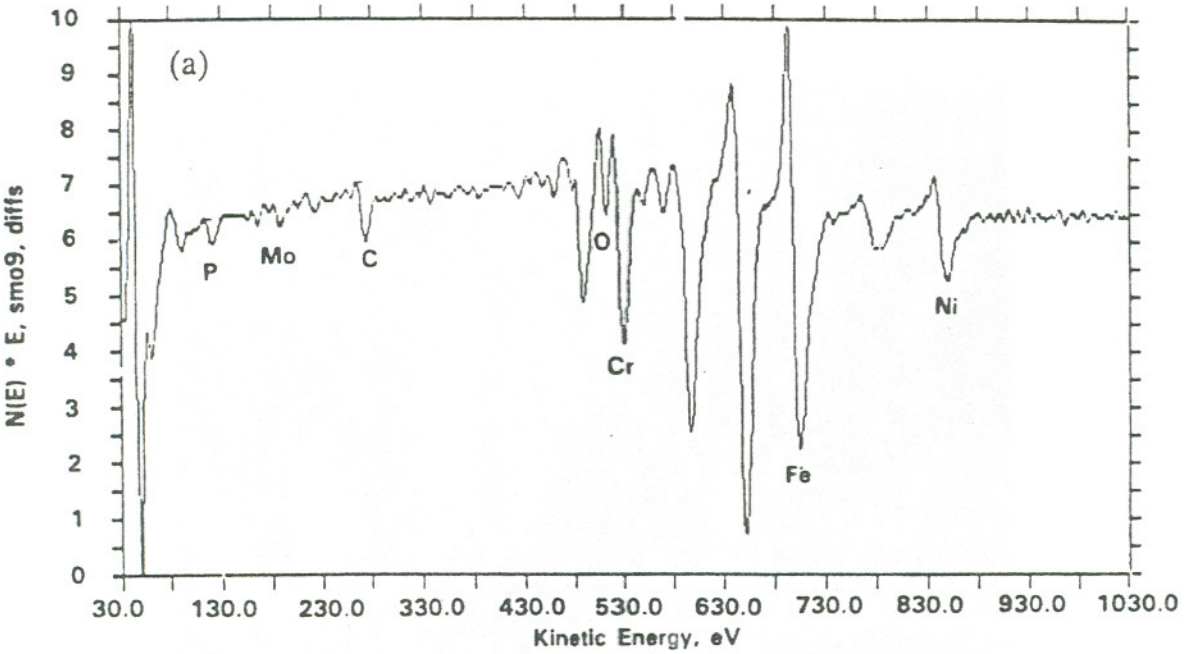

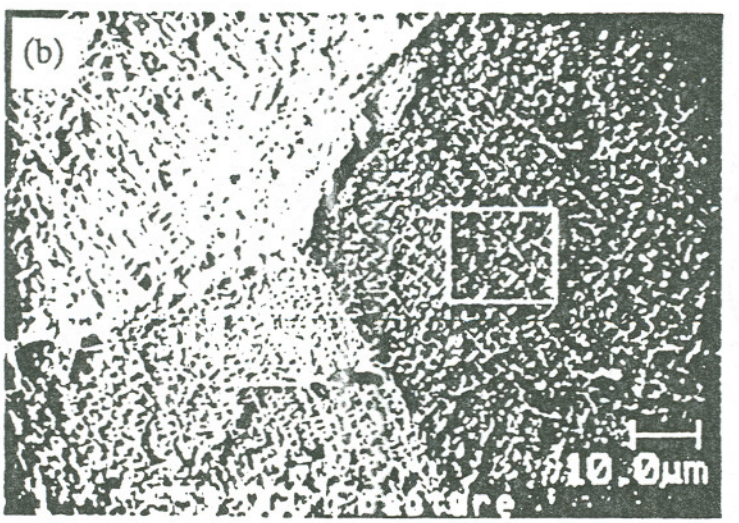

FIGURE 10. (a) Typcial AES Analysis of Phosphorus-doped 316 SS; (b) Area of Specimen Grain Boundary Scanned.

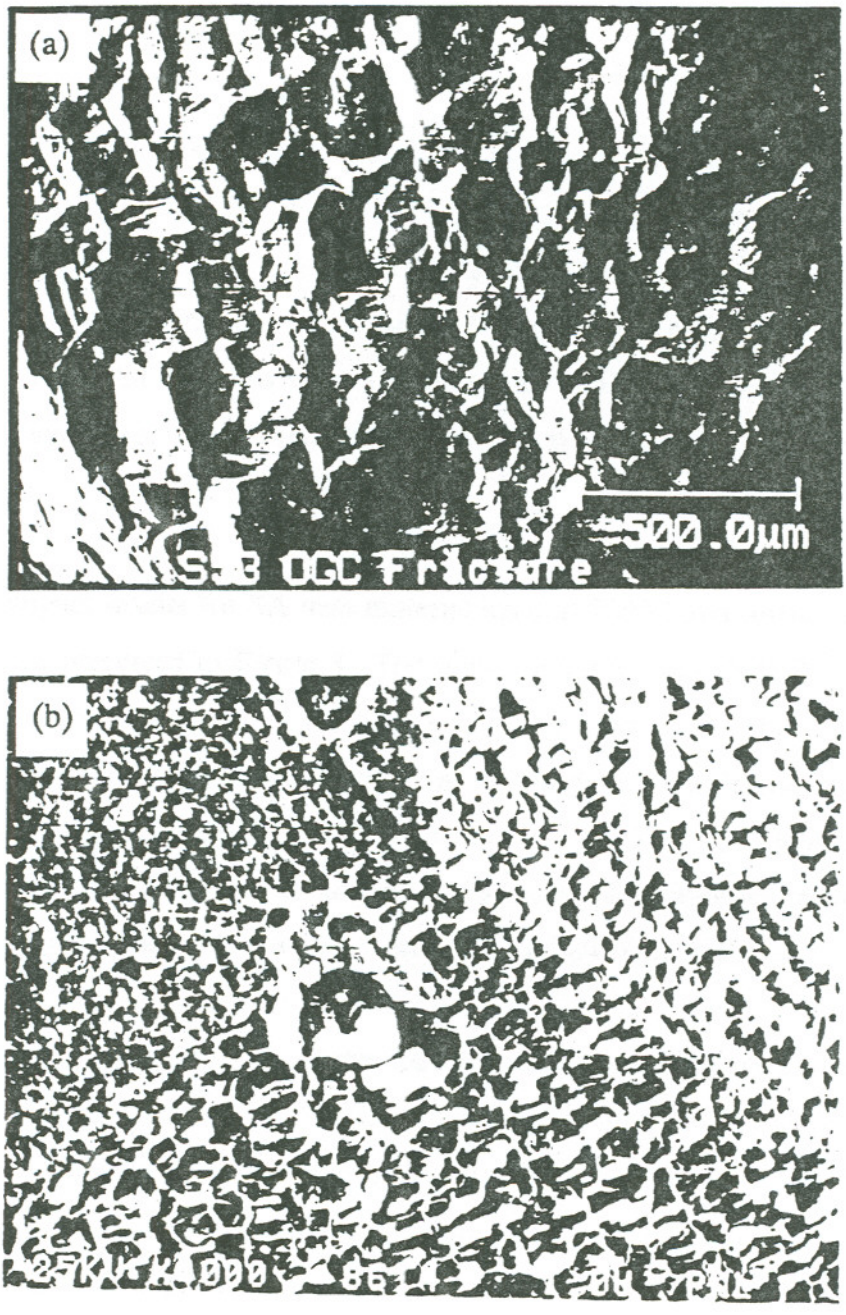

FIGURE 11. (a) High and (b) Low Magnification Fractographs of Impact Fracture Morphologies of Step-Cooled HCHP 316 SS Heats.

Effect of Carbide Precipitation

This section discusses the influence of carbide precipitation on the development of IG fracture in Type 316 SSs. This was done by studying the impact losses suffered as a function of C content. The test matrix consisted of the HCNP, HCLP and the NCHP heat. The development of IG fracture was obtained by the use of the high strain rate Charpy-V-notch impact test. All the heats were SA for 1 hour at 1100°C to achieve homogeneity and to get a uniform grain size and were then aged as function of time at various elevated temperatures.

The impact results for SA heat material aged at 750°C and impact tested at LN temperature are presented in Figure 8. The impact energy of the NCHP suffered very little degradation as a function of aging time while all heats containing C suffered substantial degradation. The impact energy for the high C heats decrease systematically as a function of aging precipitation time up to as high as 85% upon aging for 100 hours at 750°C. These results indicate that carbide precipitation plays a critical role in the low temperature embrittlement of 316 SS irrespective of the effect of P.

The fracture morphologies of the specimens broken by impact testing were subsequently studied by SEM. A change in the fracture mode from transgranular to IG was found to coincide with the drop in impact energy as illustrated in Figure 9. The observed fracture morphology change shows that carbide precipitation affects grain boundary properties and prompts low temperature embrittlement. The IG fracture increases dramatically with the resulting drop in impact toughness. Nearly 90 to 95% IG fracture is observed after 100 hours of aging at 750°C.

The LN ductile brittle transition behavior for the HCHP heat as a function of aging time at 750°C is shown in Figure 12. It illustrates the complementary behavior of the % IG fracture and the Charpy dial energy value with aging time at 750°C. The impact energy is reduced by more than 80% upon aging at 750°C, and this is accompanied by a

dramatic rise in amount of % IG fracture. The ductile-brittle transition takes place at around 1 to 5 hours at 750°C.

It is well established that carbide precipitation occurs during heat treatments at temperatures between 600 to 900°C and that the extent of carbide precipitation is proportional to the C content in these steels. All the high C heats have similar C contents; there is, therefore, a similar amount of carbide precipitation in these heats. The carbide precipitation at the grain boundaries for the HCHP heat is depicted in the TEM micrographs in Figure 13.

The impact energy drop as a function of aging time for both 750 and 800°C are presented in Figure 14. It can been seen that the impact drop is more severe at 800°C than at 750°C indicating that the carbide morphology or density, or both, developed at 800°C is more detrimental than that developed at 750°C.

Another set of experiments that emphasized the control of carbide density/morphology on fracture mode was a series of HCHP specimens tested as a function of aging temperature. The HCHP heat was aged at different temperatures for different times. The aging times were selected such that substitutional alloying elements such as Cr and P would diffuse the same distance at each temperature. Thus, diffusion distance of Cr, and presumably carbide precipitation volume, were kept constant over the range of aging temperatures by varying the time of aging. The variation in the Charpy values as a function of aging temperature for the high C high P heat is shown in Figure 15. It can be seen that the impact energy changes dramatically as a function of test temperature. The impact drop peaks out at

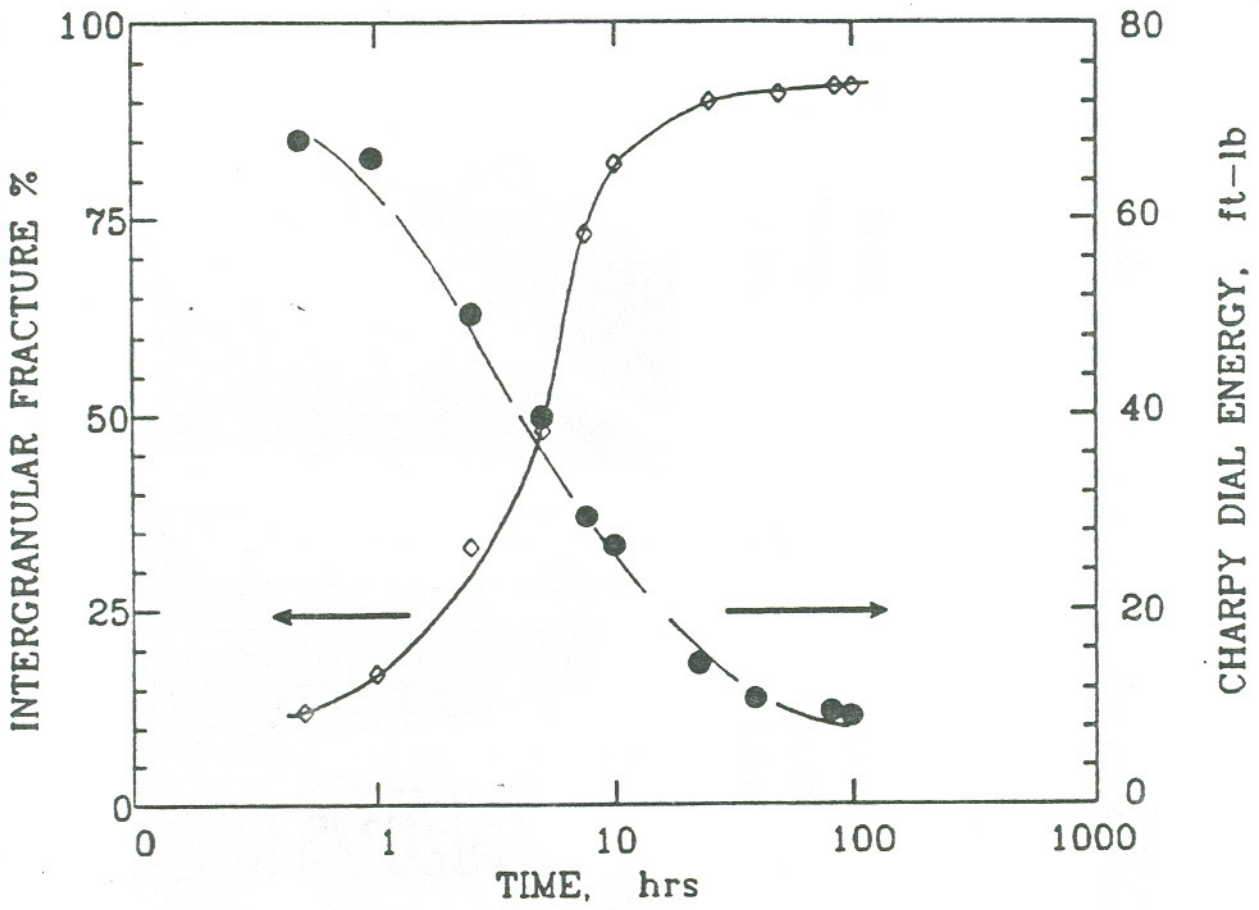

FIGURE 12. Impact Energy Ductile-Brittle Transition Behavior and Accompanying Change in Fracture Morphology as a Function of Heat Treatment Time at 750°C for the HCHP 316 SS All Heats.

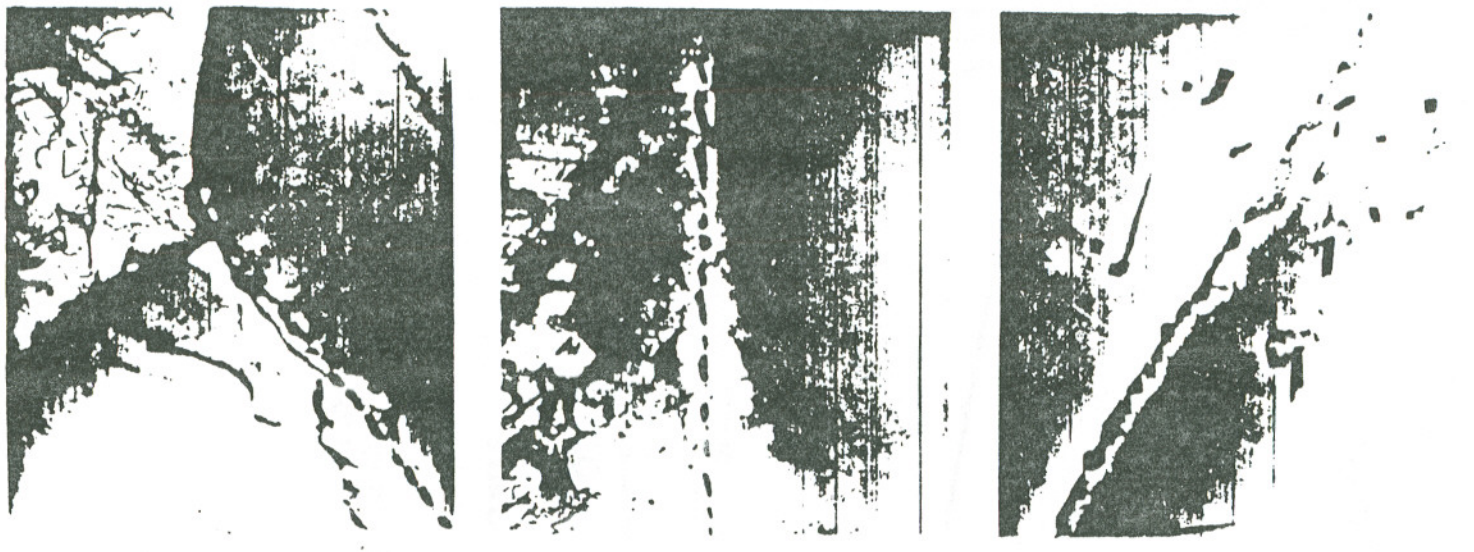

FIGURE 13. TEM Micrographs of Grain Boundary Carbide Precipitation as a Function of Aging Temperature for the HCHP 316 SS Heat.

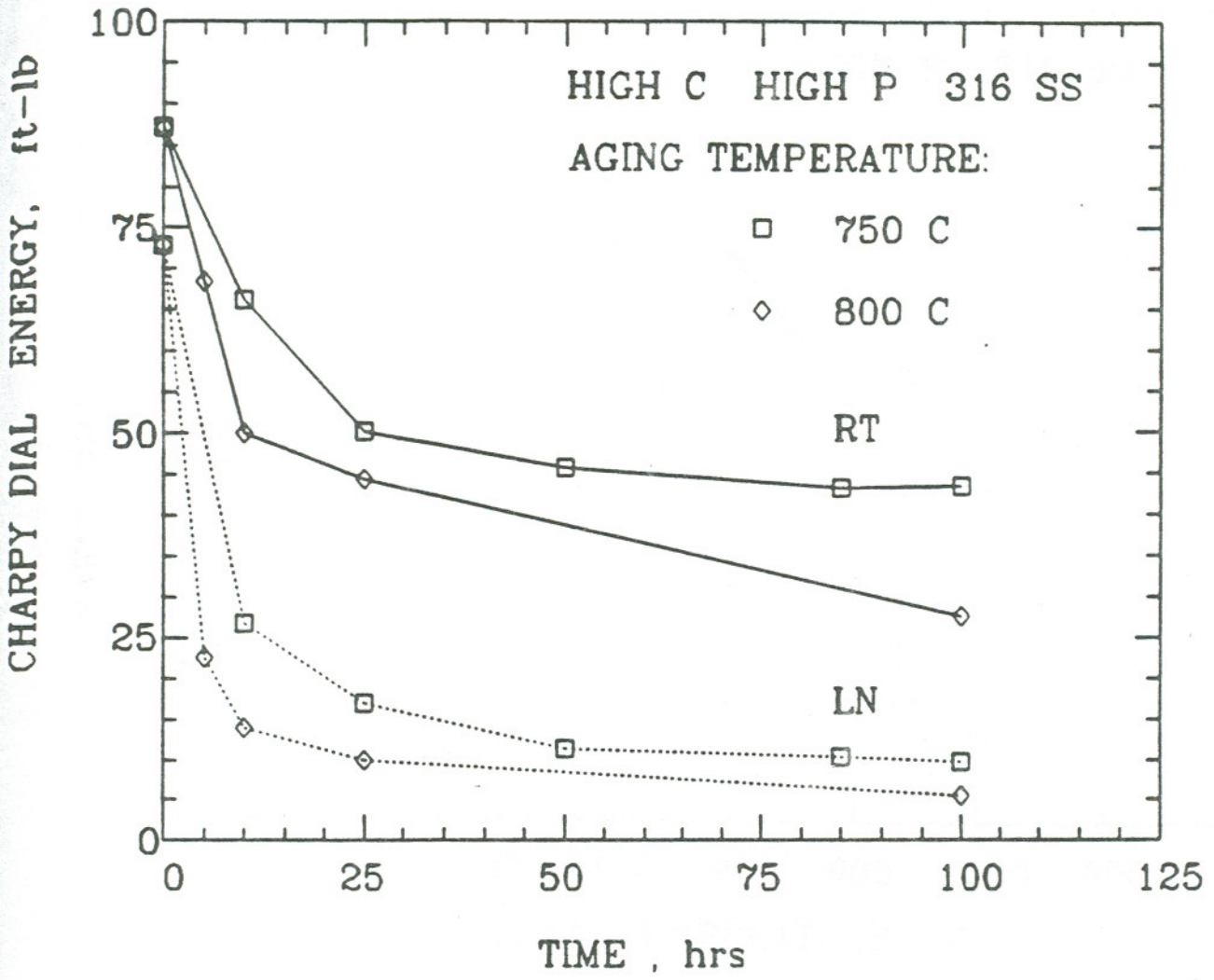

FIGURE 14. Change in Impact Energy as a Function of Aging Time and Temperature for the HCHP 316 SS Heat.

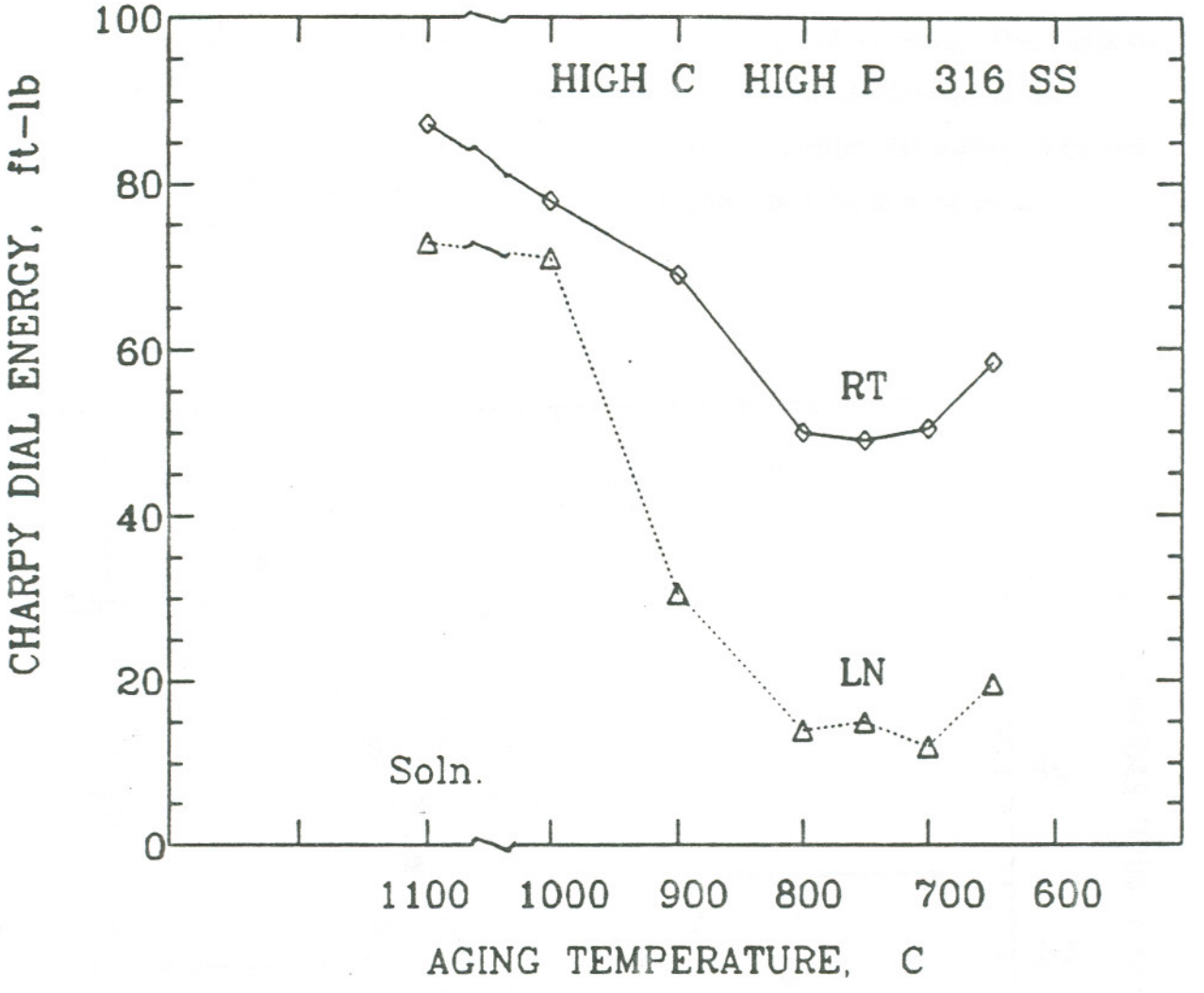

FIGURE 15. Change in Impact Energy as a Function of Aging Temperature at Constant Cr Diffusion Times for HCHP 316 SS.

a temperature of around 700°C after which the impact energy starts rising. This suggests that the effects of carbide morphology and distribution are most detrimental at that temperature. The complementary relationship between the Charpy dial energy value and the % IG fracture for the high C high P heat is illustrated as a function of aging temperature in Figure 16.

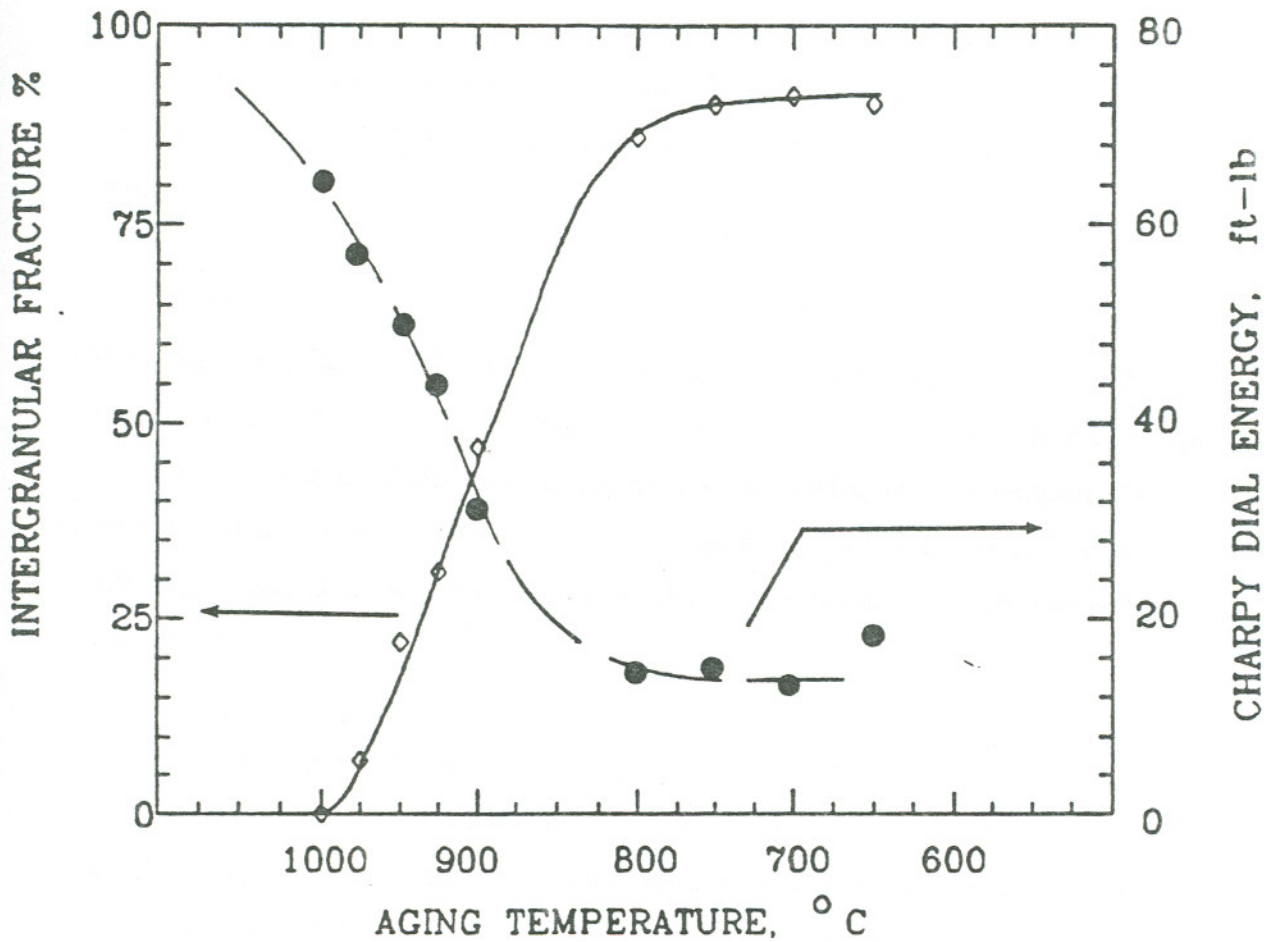

FIGURE 16. Ductile-Brittle Transition Behavior as a Function of Heat Treatment Temperature for HCHP 316 SS.

The fracture morphologies range from a ductile rupture mode at 975°C to an IG one at 750°C. Fracture morphologies of a series of specimens exhibiting impact values from 59 to 15 ft-lbs and from 7 to 90% IG failure, respectively, are presented in Figure 17.

Typical grain boundary carbide coverages for each of these treatments were estimated from TEM analysis as shown earlier in Figure 13. The carbide density can be seen to increase as the heat treatment temperature is decreased while carbide size decreases with decreasing temperatures. From Figures 13, 16, and 17 it is clear that fine, continuous carbides along boundaries are more detrimental than large well-spaced carbides.

The relationship between the development of IG fracture and the carbide coverage is depicted in Figure 18. The % IG fracture increases almost exponentially with increasing carbide coverage of the grain boundaries. This plot documents the controlling importance of grain boundary carbide coverage in promoting low-temperature IG embrittlement in 316 SS. These results are in agreement with Gan, et al.[14] It is interesting to note that these results indicate that it requires at least 30% coverage to initiate IG fracture.

The aged specimens were subjected to the EPR test to get a measure of the extent of the $M_{23}C_6$ precipitation. The IG fracture and EPR-DOS increases with increasing aging time until long aging times at 750°C where desensitization is significant and would be expected to effect EPR-DOS values, Figure 19. In this way, embrittlement in 316 SSs was again directly linked to grain boundary carbide distribution.

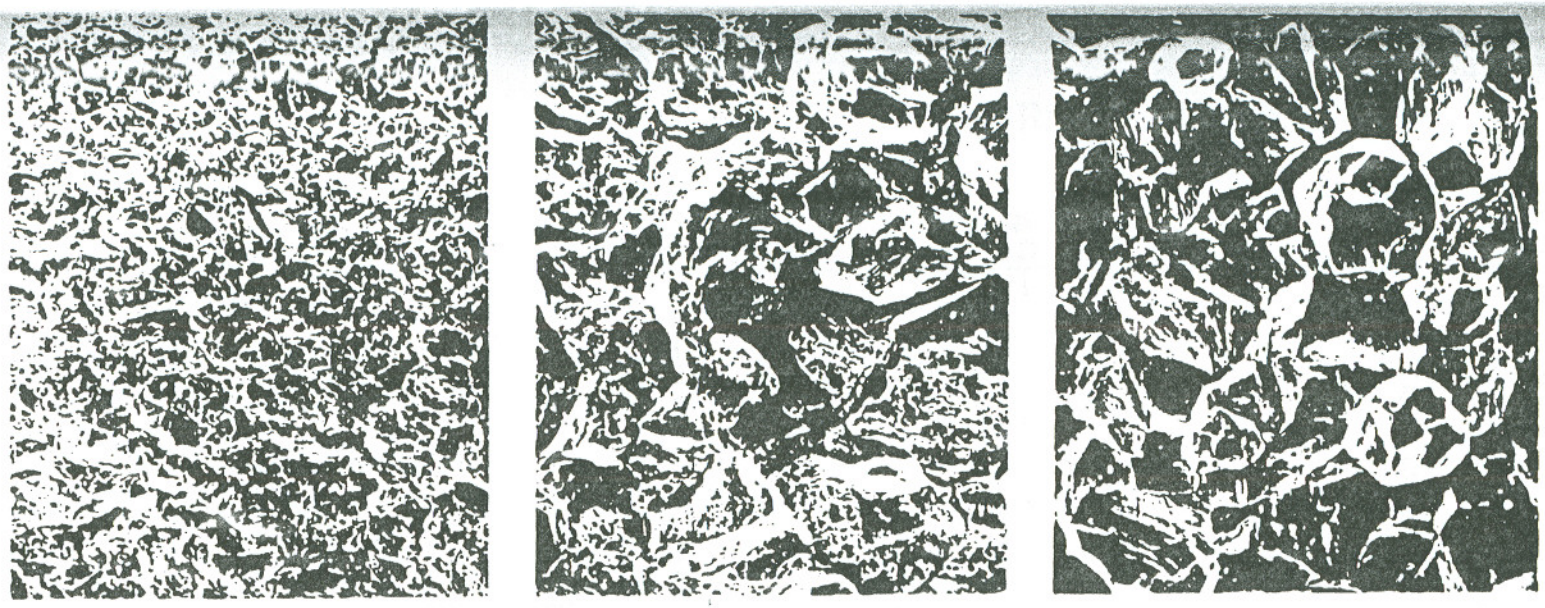

FIGURE 17. SEM Micrographs of Fracture Morphologies as a Function of Aging Temperature for HCHP 316 SS (see Figure 11 for Respective Grain Boundary Carbide Distribution Characteristics).

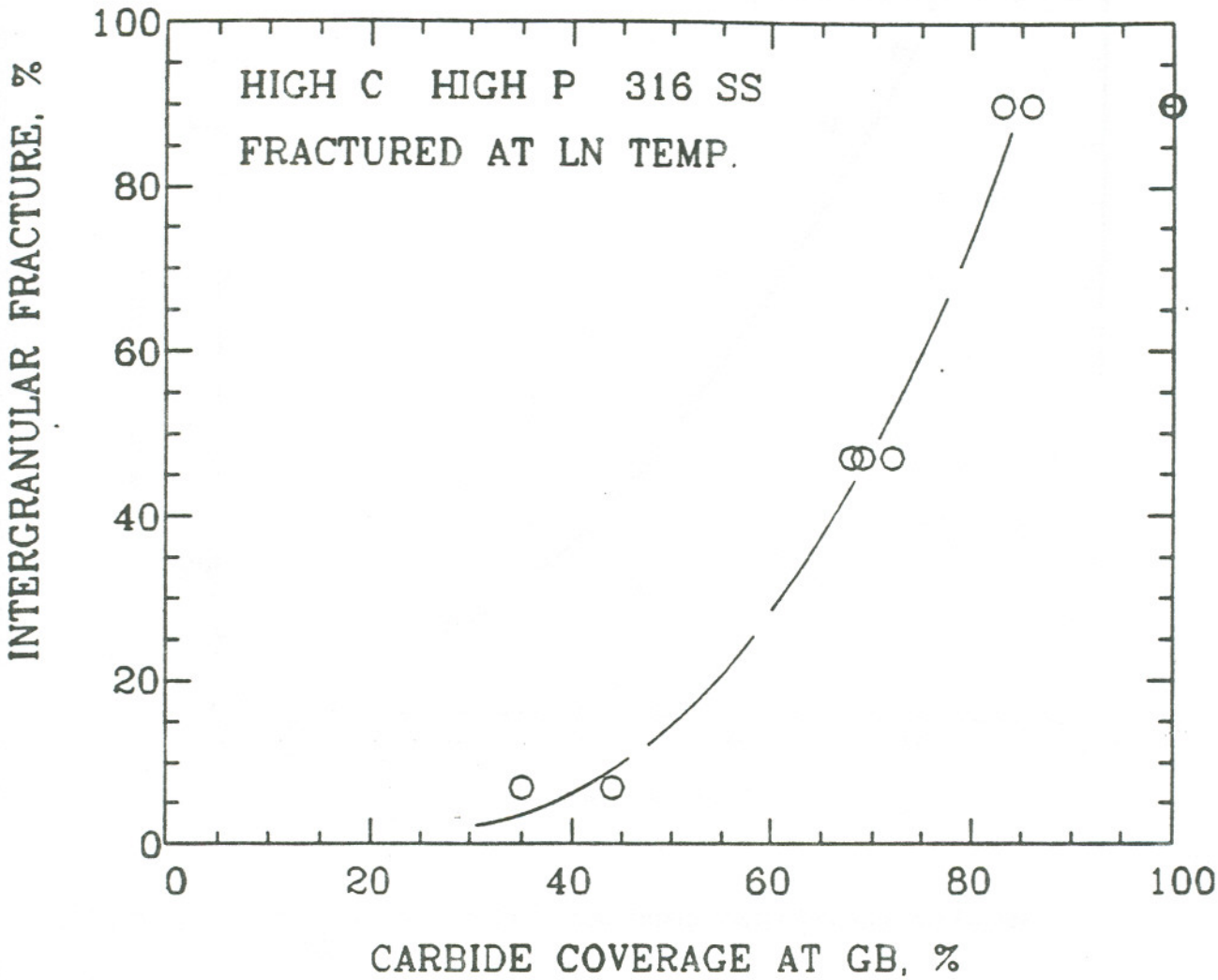

FIGURE 18. Correlation Between Grain Boundary Carbide Coverage and Intergranular Fracture for HCHP 316 SS.

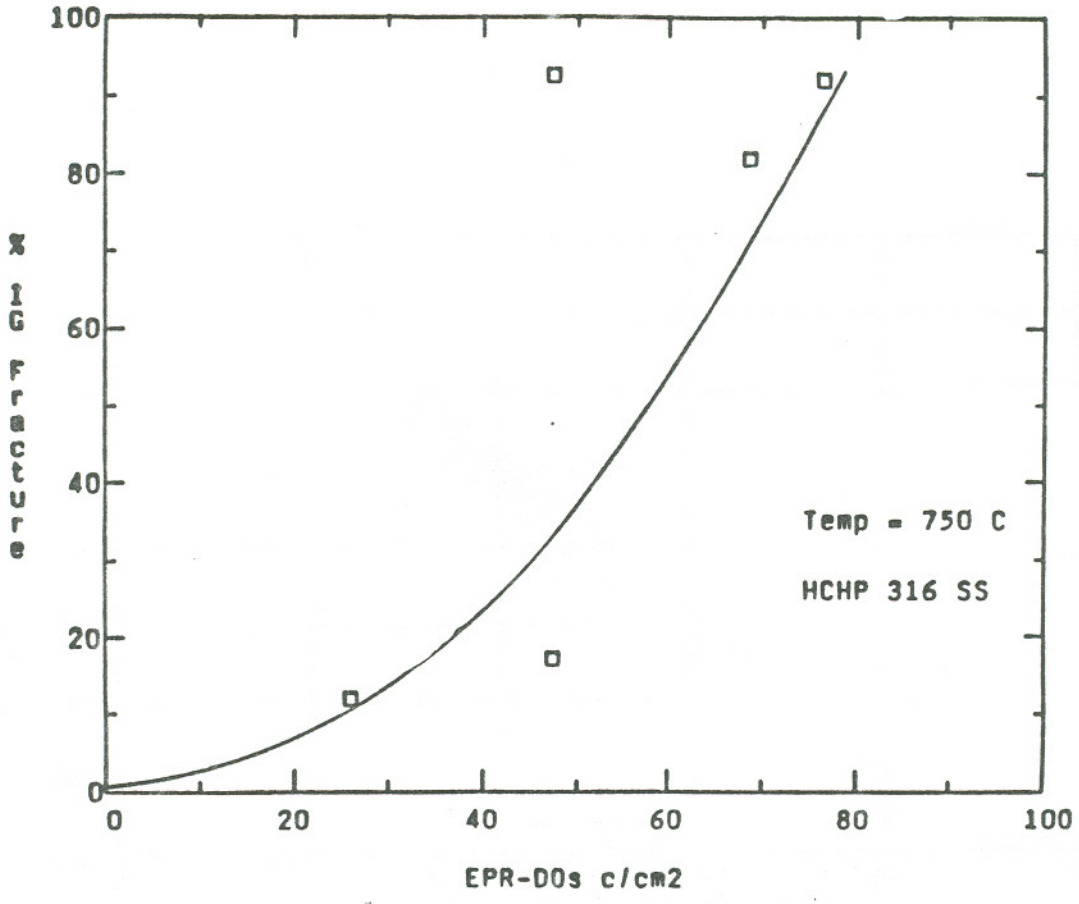

FIGURE 19. Correlation of EPR-DOS with Intergranular Fracture for HCHP 316 SS.

Effect of Grain Boundary Martensite

The following section discusses the formation of athermal martensite in the Cr depleted regions adjacent to the grain boundaries and its (potential) effect on impact toughness and on development of IG fracture. Bulk compositional correlations with martensite start temperature (M_s) suggest that athermal martensite could potentially form between room and LN temperature in highly Cr-depleted grain boundary regions of these 316 heats but not in the SA condition, see Figure 20.

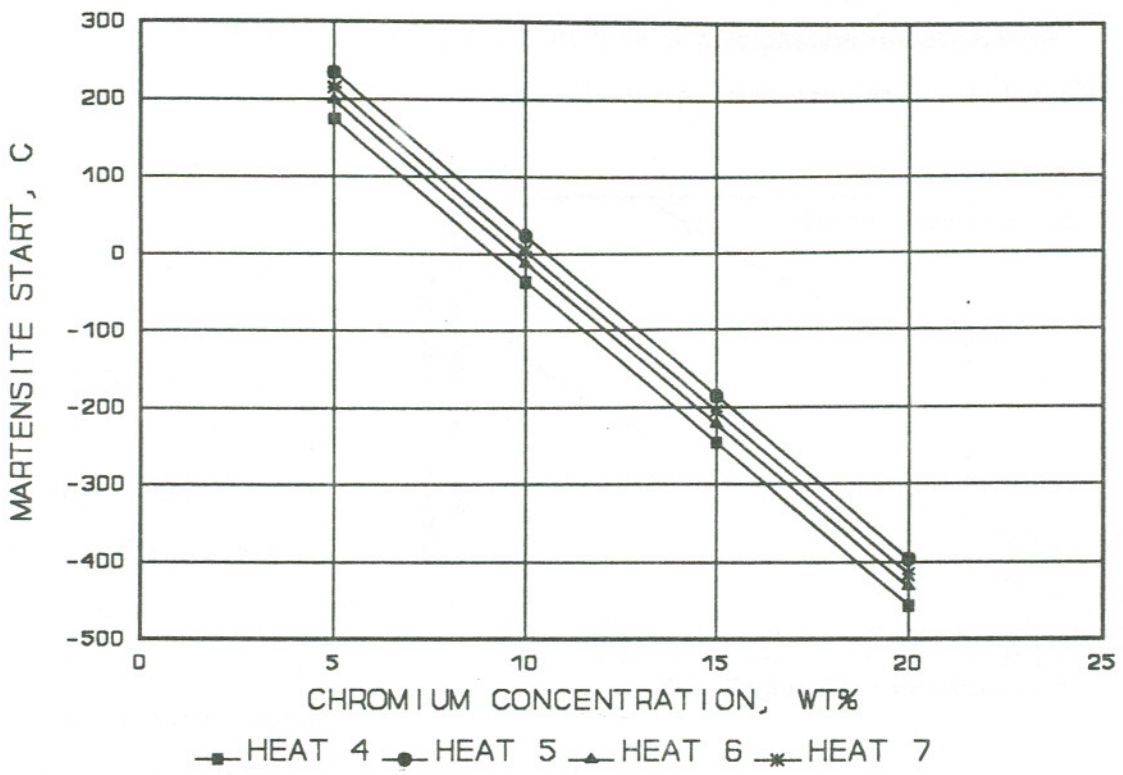

FIGURE 20. Prediction of M_s for 316 SS Heats as a Function of Cr Concentration.

The M_s temperature for SA heats with Cr contents between 16 and 17.25 wt% lie below LN temperature, -196°C, when calculated according to the formula for the M_s temperature given by Eichelman and Hull:[47]

$M_s(°C) = 1320 - 42(\%C_r) - 61(\%Ni) - 33(\%Mn) - 28(\%Si) - 1667\ (\%[C+N])$. Bulk material with Cr levels in the 8 to 10% levels, as expected in chromium depleted regions at grain boundaries, exhibit predicted M_s temperatures between -80 and +50°C, thus, martensitic transformation at LN appears possible for bulk material with compositions similar to severely Cr depleted material. The question arises as to whether transformation can readily take place in the limited confines of highly depleted material at grain boundaries.

Both the width of the Cr depleted zone and the matrix/carbide Cr minimum concentration change as a function of (isothermal) aging temperature and time. However, one can assume a fixed Cr minimum from the time of precipitation initiation until desensitization initiation. Relationships between composition, temperature and equilibrium Cr minimum, as predicted by Bruemmer, are presented in Figure 21.[35] Chromium depleted zone width at 750°C is expected to increase from about 10nm after 1 hour to more than 200nm after 100 hours with the gradient varying from the Cr minimum at the grain boundary to bulk composition at the depleted zone edge. Thus, the potential for martensitic transformation changes from a bulk effect to a complex gradient composite effect.

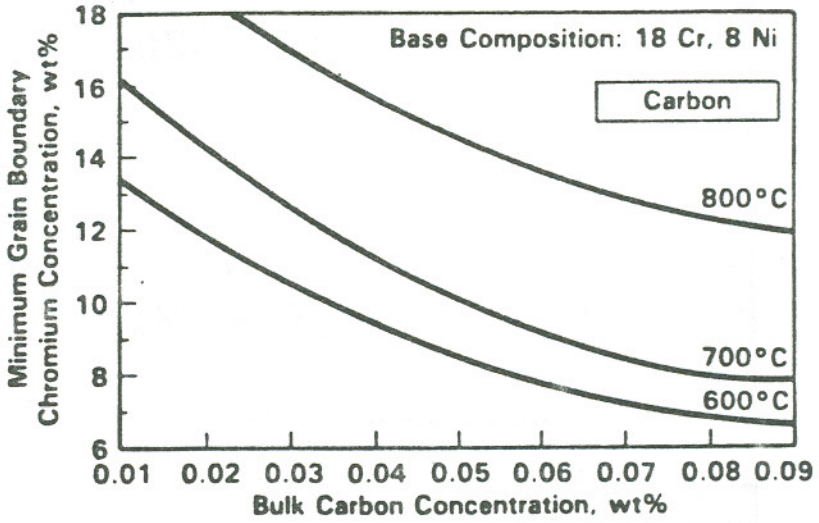

FIGURE 21. Effect of Carbon Concentration and Temperature on the Equilibrium Cr Concentration at the Carbide/Matrix Interface.

Grain boundary martensite formation has been reported to induce IG fracture in austenitic SSs at LN temperatures. The test used to confirm this hypothesis was to soak specimens at LN prior to room temperature testing and then compare these results with room temperature impact specimens tested at room temperature without the LN soak. This low temperature soak has been reported to induce α' at the grain boundaries and subsequently greatly reduce ambient temperature impact properties.[5] Figure 22 demonstrates that there is a considerable decrease in impact energy between ambient and LN specimens and that there is essentially no difference between ambient impact properties for specimens tested with and without cooling to LN. Transmission electron

microscopy examination of the specimens soaked to LN also failed to reveal any presence of α'. Thus, the presence of α' is not felt to influence the embrittlement of these steels indicating that grain boundary martensite formation is not necessary to cause significant embrittlement in Type 316 SSs.

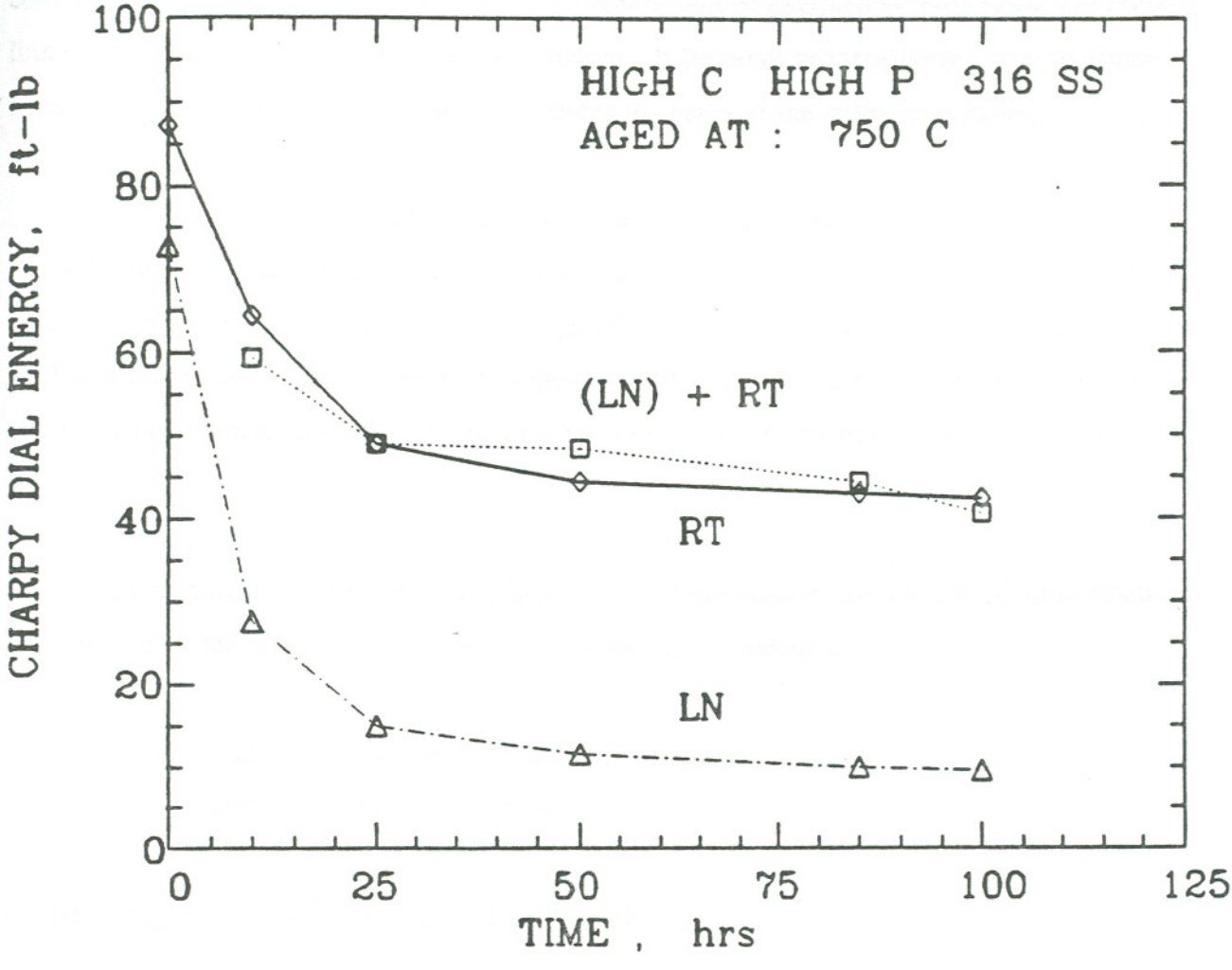

FIGURE 22. Low Temperature Exposure Effects on Embrittlement Due to Aging at 750°C for HCHP 316 SS Indicating Absence of Grain Boundary Martensite.

INTERACTION EFFECTS AND RANKING

This section gives an overview of the results obtained for the 316 SS and provides a ranking "system" of the various embrittlement mechanisms for the laboratory heats under consideration. It was shown earlier that the IG embrittlement obtained in these heats was directly linked to carbide coverage at the grain boundaries. It becomes progressively easier to obtain IG fracture in these heats as the density of carbides increases at the grain boundaries.

It can be said that P enrichments of up to 10% of a monolayer at grain boundaries did not promote significant IG embrittlement with the absence of carbides. Specimens with a high density of IG carbides with or without P segregation, were embrittled. The independent effect of P was relatively small. However, P segregation may reduce the energy required for fracture of the carbide/matrix interface. Formation of grain boundary martensite was not observed in these heats.

In conclusion, for the laboratory heats under consideration, the various IG embrittlement mechanisms in the order of decreasing potency would be ranked as:

- Grain boundary carbide precipitation
- Grain boundary P segregation

EMBRITTLEMENT MECHANISMS IN TYPE 304 SS

This section discusses the influence of the following potentially harmful embrittlement mechanisms:

- Grain boundary carbide precipitation
- Grain boundary P segregation
- Grain boundary martensite formation
- Transgranular and grain boundary sigma phase formation

This study was performed by using three laboratory heats with the same base chemistries except for the C and P contents, they were HCHP, MCLP and LCHP heat. The data presented in each subsection is aimed at isolation, evaluation and comparison of the individual and relative effects of each of these embrittlement mechanisms.

Effect of Sigma Phase Formation

The 304 SS heats were heat treated essentially the same as those discussed in the 316 SS section. They were subjected to a solution heat treatment at 1100°C for 1 hour and then aged for various times at 700°C. All heats except the LCHP heat exhibited results similar to the 316 SS heats, as discussed in the following sections. The LCHP heat behaved abnormally and was, therefore, subjected to additional scrutiny.

The first surprising observation connected with the LCHP heat was that it exhibited reduced Charpy energy at very short aging times at 700°C, Figure 23. The second unexpected observation was that this reduction in impact energy was related to a transgranular failure mode.

The fracture surfaces showed no evidence of IG fracture associated with the drop in the impact energy. For the most part, the fracture seemed to be of a ductile type although some regions showed a rupturing tendency. Figure 24, in particular, illustrates the basically transgranular nature of this failure as well as the apparent multiple directions of the crack propagation. The crack seems to change direction frequently, as if following the path of least resistance, sometimes travelling perpendicular to the notch towards a brittle region. The SEM micrograph of the same region at a higher magnification indicates the possible existence of a brittle phase.

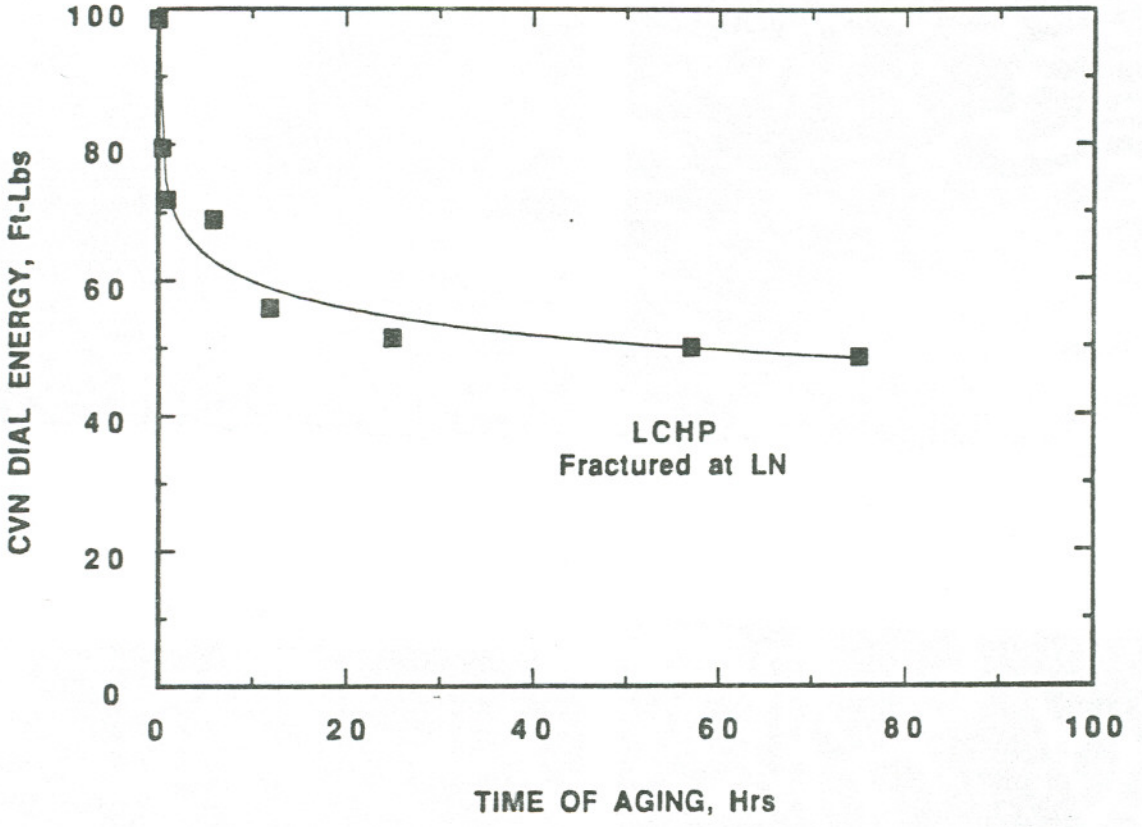

FIGURE 23. Reduction in Impact Energy as a Function of Heat Treatment Time at 700°C for LCHP 304 SS Solution Heat Treated at 1100°C for 1 Hour.

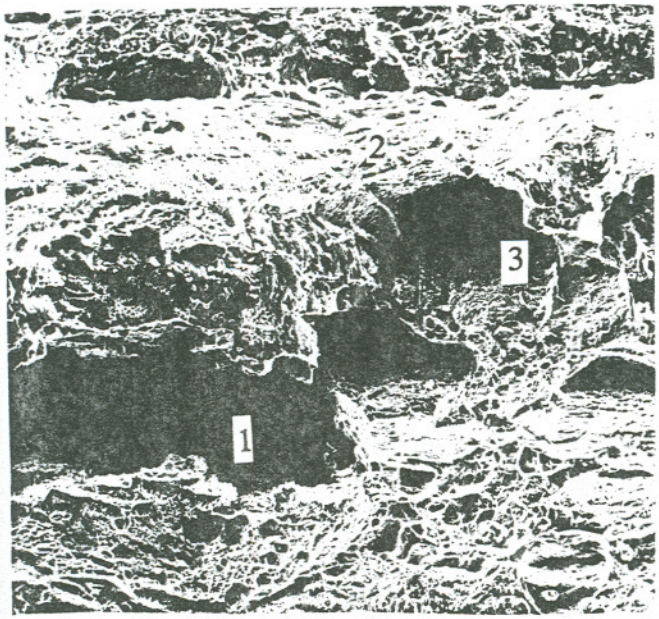

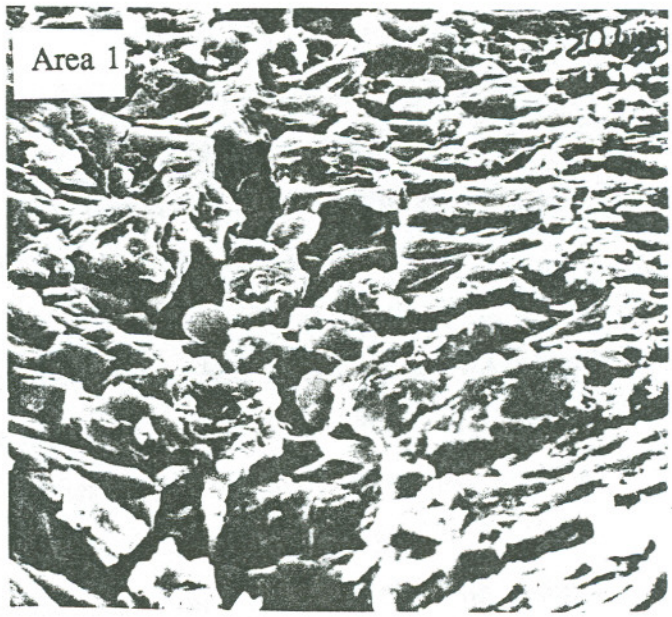

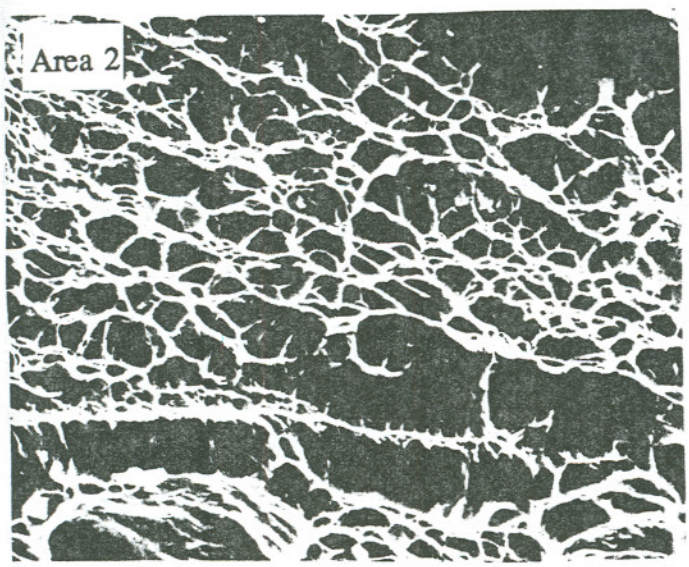

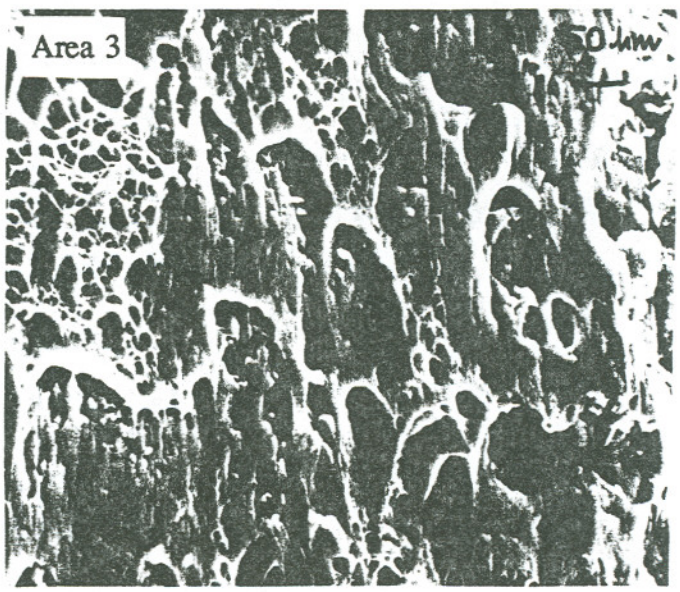

FIGURE 24. SEM Micrographs of Fracture Surfaces of LCHP 304 Indicating Direction of Crack Propagation Around Sigma Phase.

Danyluk, et al also reported this type of "fast" embrittlement and the associated transgranular failure mode.[2,7,11] However, it was hypothesized to be associated with the presence of transgranular iron phosphide precipitates in an alloy containing a supersaturation of P. In addition, no metallographic analysis was presented to back up this finding.

Metallographic analysis of the LCHP heat after solution heat treatment at 1100°C and aging at 700°C was undertaken, and resulted in identification of both delta and sigma phase. A variety of etching reagents have been specified in the literature to identify the presence of delta-ferrite and sigma phase; 10N KOH was used in this study. Electrolytic etching with 10N KOH colors the delta-ferrite reddish brown and the sigma-phase blue.[56] The delta-ferrite show a characteristic sharp angular outline and the eutectoid transformation of delta-ferrite produces a morphological change to a more-rounded sigma.

Figures 25 and 26 show optical micrographs of the etching action of 10N KOH on the solution heat treated and the aged samples. The sigma particles can be seen to form at the ferrite-austenite boundary and then grow into the ferrite region. An Energy Dispersive X-ray Microanalysis confirmed the presence of the sigma regions as the measured Fe, Cr and Ni wt% were 61.2, 28.8, and 5.8, respectively as compared to the expected wt% of 61, 29, and 5.8, respectively.[57] Sigma formation from delta-ferrite usually occurs in the form of a lamellar structure. This is borne out from the micrographs in Figure 27 which shows SEM micrographs of the etched sigma indicating a lamellar structure which is formed by the simultaneous growth of sigma and austenite into the delta-ferrite.

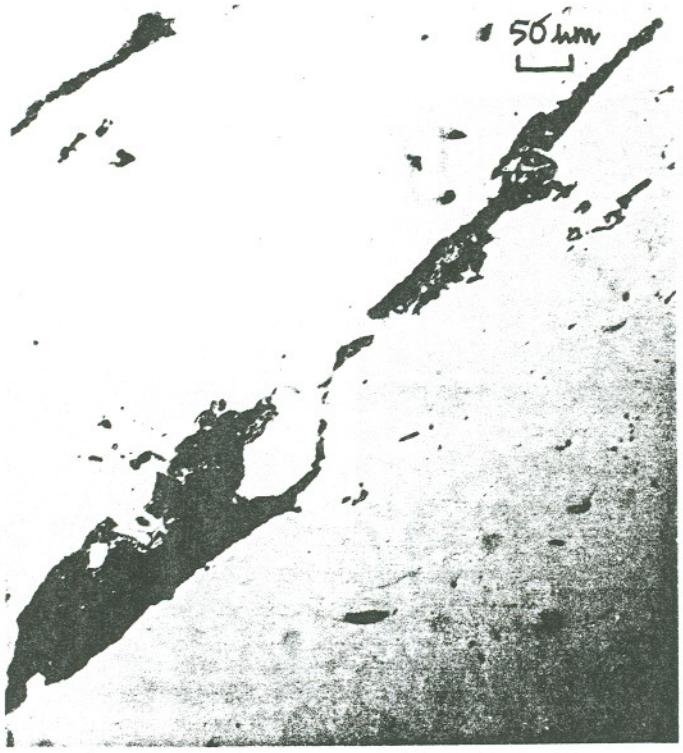

FIGURE 25. Optical Micrograph of Specimen Subjected to 10N KOH Etch Revealing Sigma Phase in LCHP 304 SS.

FIGURE 26. Optical Micrograph of specimen subjected to 10N KOH Etch Revealing Delta-Ferrite in LCHP 304 SS.

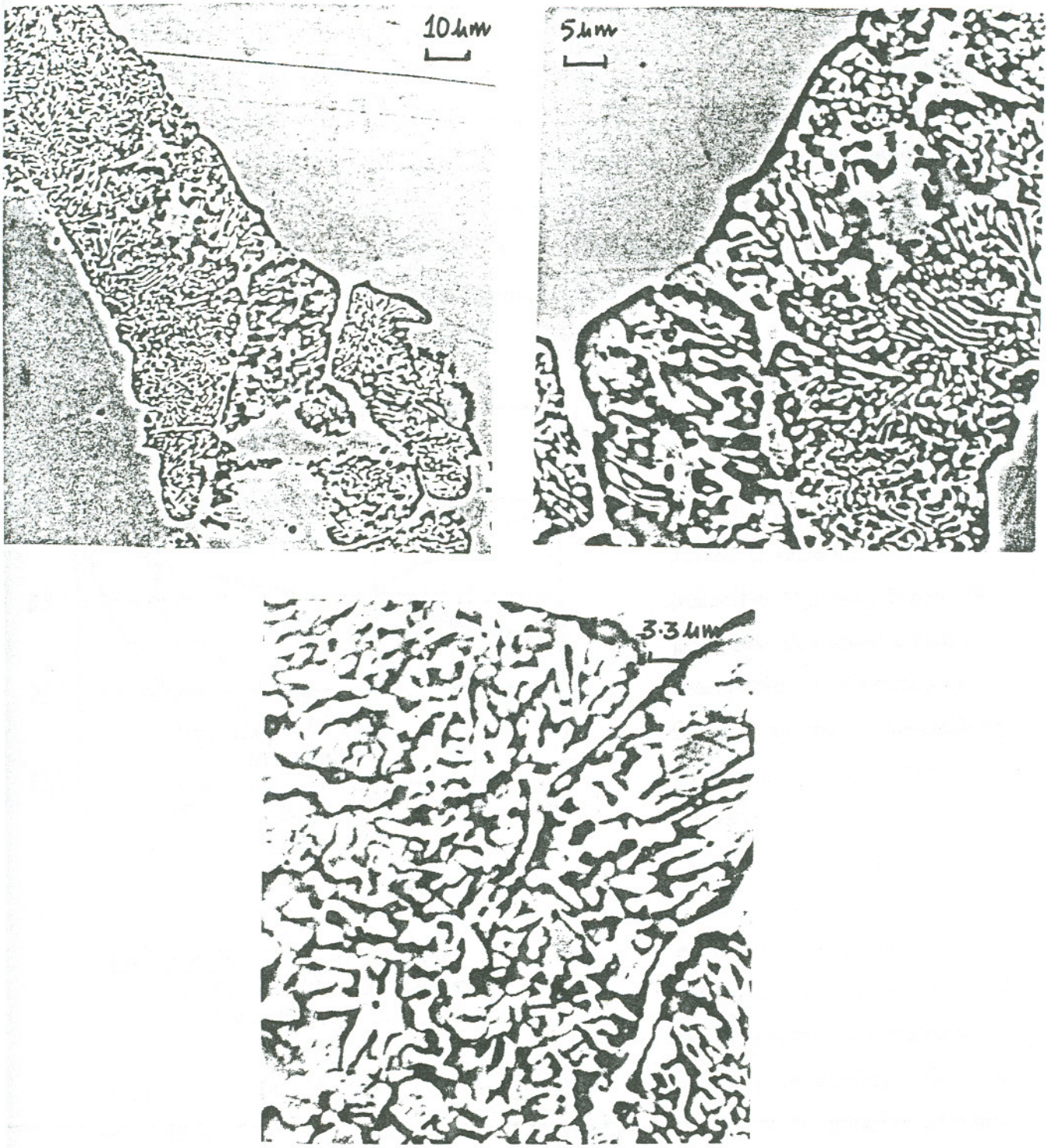

FIGURE 27. SEM Micrographs of Specimen Subjected to 10N KOH Etch Illustrating the Lamellar Structure of Sigma Phase.

Sigma phase can form directly from the austenite phase in susceptible SSs but this process requires much longer times at aging temperatures than these heats were subjected to. Sigma phase can form at relatively short aging times in the presence of retained delta, as found in this heat and illustrated in Figure 28. The mechanism for the formation of the lamellar sigma structure is that initial sigma precipitation depletes the adjacent matrix of both Cr and other ferrite-stabilizing elements. The C and other austenizing elements diffuse quickly through the ferrite and a Cr gradient is formed which adjusts the local chemistry favoring a stable austenite region.

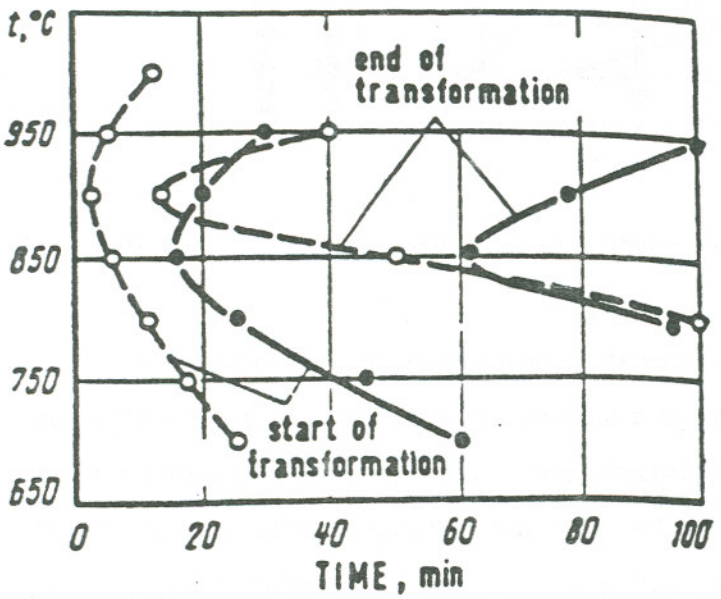

FIGURE 28. Diagram Illustrating Isothermal Decomposition of Delta-Ferrite.

Many authors have developed empirical equations for the possibility of existence of ferrite as a second phase in an austenitic material. The Schaeffler Diagram, Figure 29, gives one idea about a heat's susceptibility to formation of ferrite in as-cast SS materials by an estimate of the relative potency of the austenite stabilizers and the ferrite formers i.e., the nickel and the Cr equivalents, respectively.[58] Figure 29 shows that ferrite could possibly form from the bulk composition of the LCHP heat (%Ni = 15.005 and %Cr = 21.43). Accordingly, the bulk composition of the LCHP heat was found to make it susceptible to the presence of delta-ferrite.

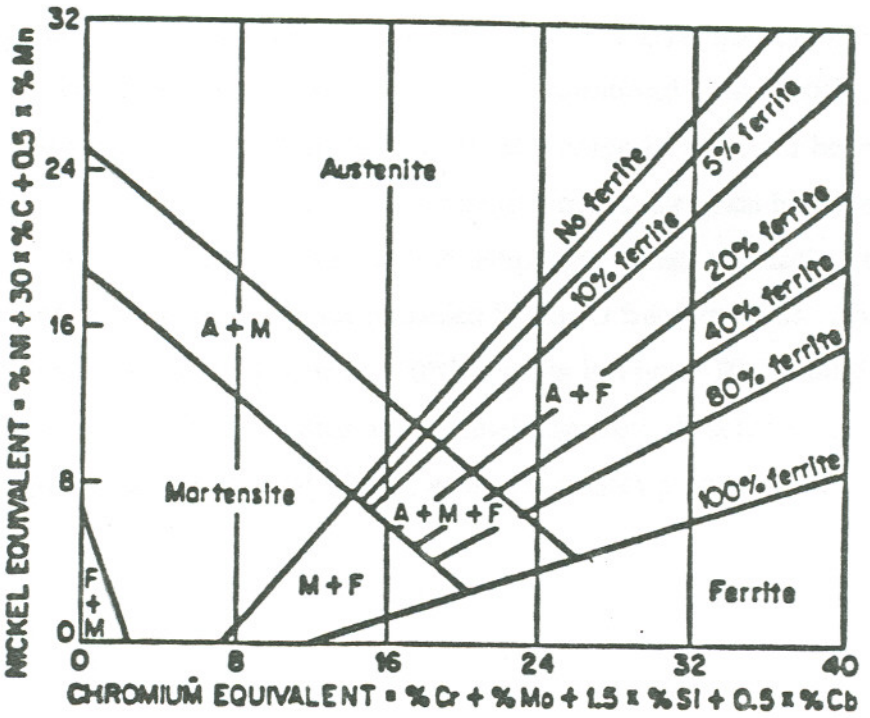

FIGURE 29. As-Cast Schaeffler Diagram Phase Stability Predictions for SS Weld Deposits.[58]

Even though delta-ferrite was to be expected in the as-cast structure it was expected that subsequent hot deformation would eliminate it in the wrought material. It is hypothesized that the presence of delta-ferrite in this experimental alloy was due to a lack of sufficient hot deformation included recrystallization and insufficient high temperature substitutional diffusion times. It is felt all delta-ferrite could have been removed from this alloy if it had been subjected to a modified hot rolling treatment sequence.

The presence of delta/sigma and sigma phase effect on impact properties obviously would be expected to mask any effect of the presence of P on the grain boundaries. Thus a series of high temperature homogenization heat treatments were undertaken to dissolve the delta-ferrite, as the metastable retained delta-ferrite transforms to austenite if held at high temperature long enough.

A 6 hour SA treatment at 1210°C results in partial dissolution of the delta-ferrite. The

grain size after the above SA treatment corresponded to ASTM grain size number 2.6. During the recrystallization and growth process, however, the undissolved delta-ferrite stringers were intersected by the growing grains and produce a partial pinning of the grain boundaries. As a result, upon further aging at 700°C, the undissolved delta-ferrite at the grain boundaries transform to sigma, again at fairly short aging times at this temperature, and produce a drop in impact toughness. This drop in toughness was accompanied by an IG fracture mode. The variation of impact energy as a function of aging time at 700°C is given in Figure 30. A third solution heat treatment of 12 hours at 1100°C resulted in essential complete dissolution of delta without accelerated grain growth and with little, if any, effect on impact properties with aging time at 700°C.

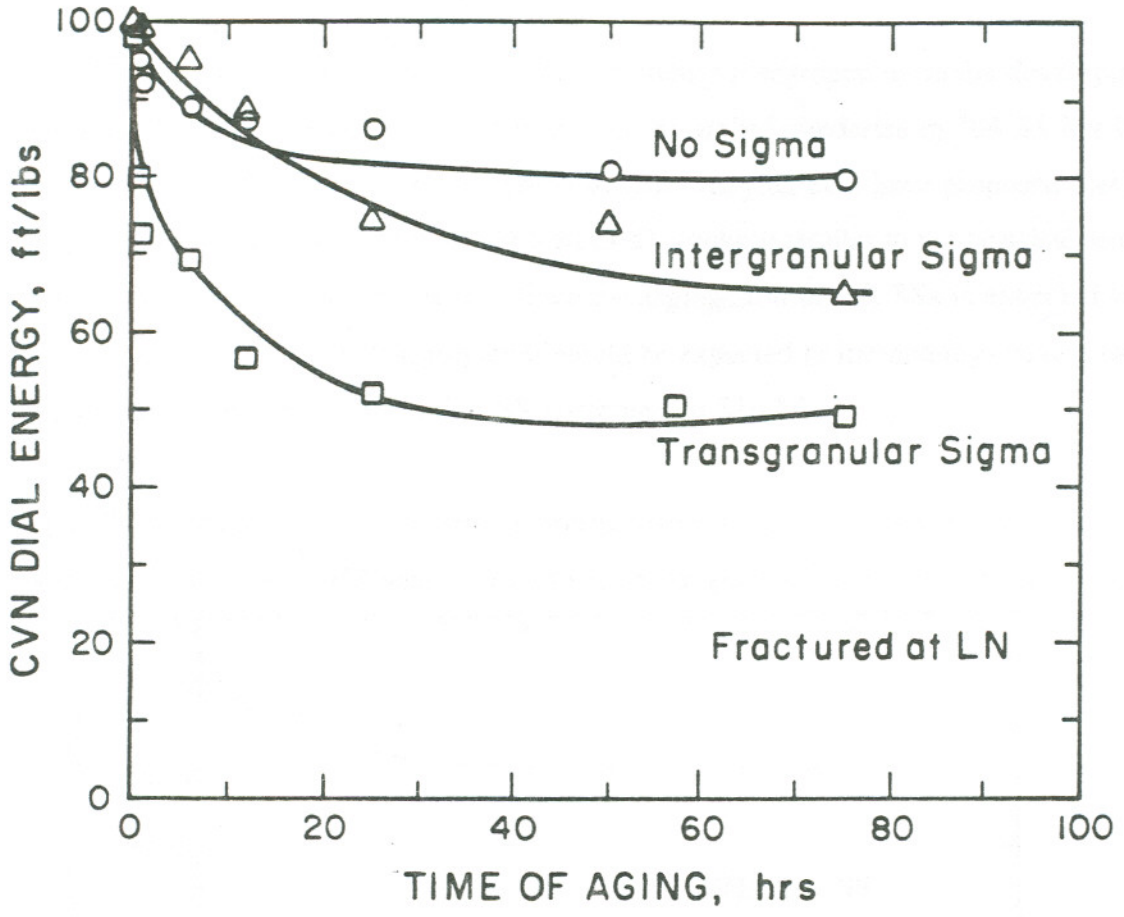

FIGURE 30. Reduction in Impact Energy for LCHP 304 SS due to Formation of Intergranular and Transgranular Sigma as a Function of Solution Anneal Treatment.

Thus, the presence of sigma phase has been shown to be a potential embrittling agent whether present in an IG or transgranular mode. All LCHP alloy subjected to further analysis, as discussion in the following section, was given the 1100°C - 12-hour solution annealing treatment in order to minimize/eliminate the detrimental effect of sigma.

Effect of Grain Boundary Phosphorus Segregation

This section addresses the influence of grain boundary P segregation on the development of IG fracture in 304 SS. Phosphorus concentration at the grain boundaries in 304 SS has been reported to be markedly higher than the bulk composition. Danyluk et al have proposed that this impurity segregation to grain boundaries could lead to IG cracking similar to the classical temper embrittlement observed in low alloy steels.[7] Since the segregation in 304 SSs is expected to be of a higher order that the 316 SSs, P segregation would be expected to (potentially) have a larger role to play in the IG embrittlement of 304 SS compared to 316 SS.

Figure 31 illustrates the drop in impact energy tested at LN temperature as a function of aging time at 700°C for the LCHP heat. Loss in impact toughness is very small in this heat in

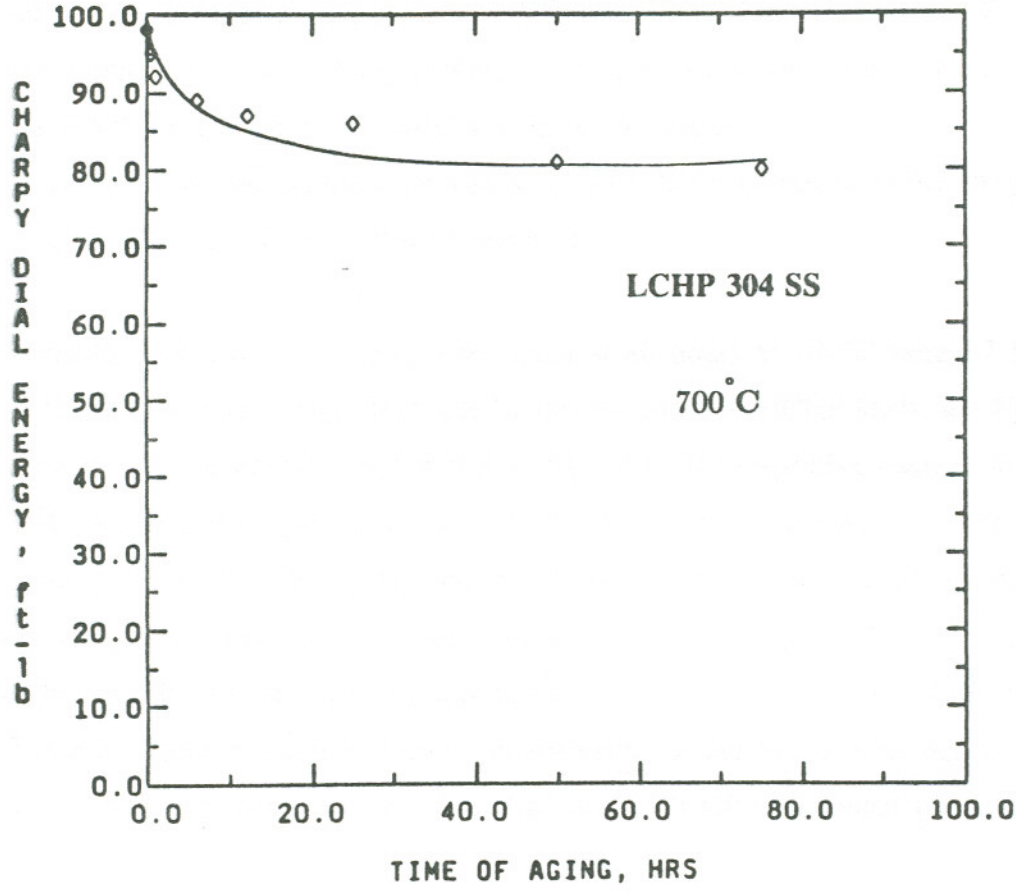

FIGURE 31. Reduction in Impact Energy as a Function of Heat Treatment Time at 700°C for LCHP 304 SS.

which the major embrittlement mechanism under consideration is P segregation. This heat suffers a drop of 20 ft-lbs upon aging at 700°C. This slight drop in impact energy could be either due to the segregated P, carbide precipitation and/or residual (delta) sigma phase. The fracture morphologies remained mainly transgranular. There was no significant IG cracking observed at

LN testing. Thus, P segregation, for the amount segregated in the heats under consideration is not effective at promoting IG failure under high strain rate conditions.

The MCLP heat exhibited considerably greater reduction of impact energy than the LCHP heat as a function of aging at 700°C, Figure 31. In addition, the MCLP heat fracture surfaces exhibited substantial IG fracture. These results indicate that the presence of P is not needed to induce grain boundary embrittlement. Comparison of the LCHP, MCLP and HCHP results in Figure 31 indicates that impact energy decreases as C content increases, but do not rule out a (secondary) effect of P.

A second set of heat treatments oriented towards assessing the effect of P on grain boundary embrittlement consisted of step cooling. A stepped heat treatment of 12 hours at 700°C + 50 hours at 600°C + 100 hours at 500°C was done to maximize P segregation to the grain boundaries. The time at each temperature was so chosen that it corresponded to the expected equilibrium segregation time for P at that temperature.

The resultant LN impact energies after aging at 80 hours at 700°C were 87 ft-lbs for LCHP, 68 ft-lbs for Medium C-High P (MCHP), and 30 ft-lbs for HCHP heats, see Figure 32. All of these values are considerably higher than exhibited by the respective heats at long aging times at 700°C, where carbide growth is expected to be maximized, Figure 32. This indicates that maximization of carbide precipitates, and not P segregation, is the controlling mechanism for grain boundary embrittlement. It is interesting to note that measured grain boundary P content for the HCHP heat step cooled was twice that measured for a 700°C/½ hour heat treatment, Table 5. The measured P grain boundary value for the MCLP heat step cooled was approximately an order of magnitude less than that for the HCHP step cooled specimen.

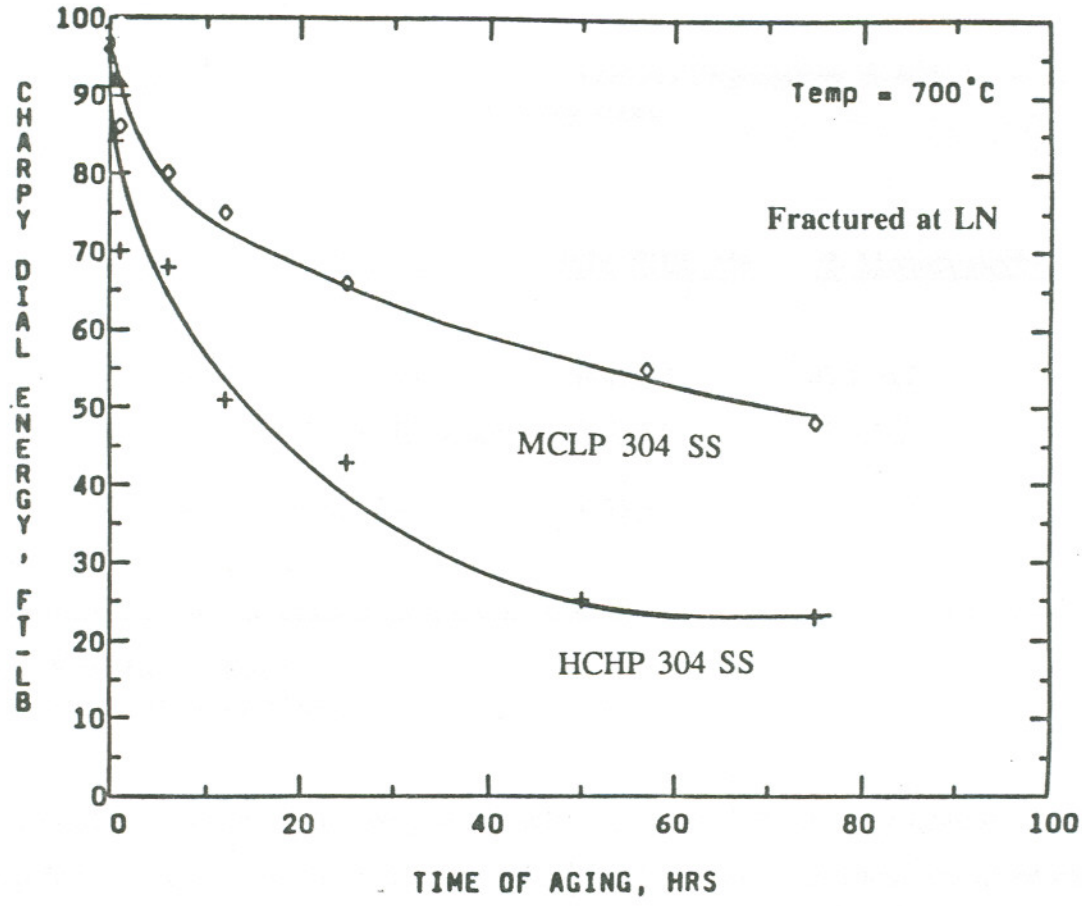

FIGURE 32. Reduction in Impact Energy for MCLP and HCHP Heats as a Function of Aging Time at 700°C for a Step Heat Treatment of 12 Hours at 700°C + 50 Hours at 600°C + 100 Hours at 500°C.

TABLE 5. Grain Boundary Phosphorus Segregation in 304 Laboratory Heats

Heat Number	Type	Heat Treatment	P/Fe PHR, *%	% Monolayers**
1	MCLP	Step Cool	0-1, 0.1	0-1, 0.2
2	HCHP	700°C/12 hours	3-7, 5.8	3-5,4.2
3	HCHP	Step Cool	8-18,12	7-12,8.8

* PHR = Peak Height Ratio
** Range and Average of Measured Levels are Listed.

A third set of experiments designed to accentuate the effect of P segregation effects over carbide precipitation consisted of long time aging at 500°C. This treatment would be expected to minimize carbide nucleation/growth due to low Cr diffusivity but still allow achievement of close to equilibrium P at grain boundaries.

The MCLP and the HCHP were subjected to isothermal aging treatments at 500°C, as a function of time. Neither of the two heats registered any major drop in impact energy up to 100 hours exposure time, Table 6; this is presumably due to the relatively slow rate of $M_{23}C_6$ precipitation in these heats at 500°C. These results reinforce the observation that P alone plays a secondary role to C as an embrittling mechanisms. These latter tests are important to these observation as they maximize P while minimizing carbide nucleation/growth for the medium and high C heats.

One unexpected result of this study was the "low" segregated P levels detected at the HCHP grain boundaries, Table 6. Briant et al[59] had previously reported a maximum P to Fe peak height ratio of 30 to 40% as a measure of P segregation for a 50 hour aging period at 700°C in

304 SS. Measurements of segregation for these laboratory heats showed a maximum P segregation of the order of 8 to 18% after step cooling treatment, which was expected to exhibit more P segregation than a

TABLE 6. CVN Impact Energy Values for HCHP and MCLP 304 SS at 500°C.

Number	Heat	Time of Aging,hrs	CVN Dial Energy,ft-lbs
1	HCHP	12	96
2	HCHP	50	88
3	HCHP	100	79
4	MCLP	12	98
5	MCLP	50	90
6	MCLP	100	84

100 hour soak at 700°C. The question thus arises as to whether an increase in P at the grain boundaries would induce substantial embrittlement. It is unclear whether the lack of % IG fracture is due to the low amount of grain boundary P segregation or due to the ineffectiveness of grain boundary P segregation to act as an embrittling agent. The data does indicate, however, that there need not be segregated P present at the grain boundaries to induce IG fracture under high strain rate conditions in 304 SS and that P levels up to 8 to 18% of a monolayer does, by itself, induce significant embrittlement.

Effect of Grain Boundary Carbide Precipitation

This section discusses the influence of grain boundary carbide precipitation as an IG embrittling mechanism in 304 SS. This will be done by presenting the impact losses suffered

as a function of C content. The test matrix consisted of the HCHP, MCLP and LCHP heats. Intergranular fracture was accentuated by the use of a high strain rate test, namely the Charpy impact test. All heats were SA for appropriate times to achieve a homogeneous and uniform microstructure. The as-rolled MCHP heat was SA for 2 hours at 1100°C. The HCHP heat was SA for 1 hour at 1100°C. The LCHP heat was SA for 12 hours at 1100°C, see Table 2 for heat SA grain sizes.

After the SA treatments, the heats were isothermal aged at a variety of temperatures, as a function of time. The variation in LN impact energy as a function of aging time at 700°C for these heats is presented in Figure 33. The impact energies of the LCHP heat suffer very little degradation as a function of aging time while all heats containing C suffered substantial degradation with degradation increasing with increasing C content. The impact energies of the MCLP heat decreases systematically as a function of aging time and is reduced by almost 50% to (48 ft-lbs) after aging 75 hours at 700°C while the HCHP heat drops by almost 85% after 75 hours at 700°C.

The fracture morphologies of the specimens broken by impact testing were subsequently studied by SEM. The fracture morphologies range from a transgranular mode for the SA material and LCHP heat to an IG mode for MCLP and HCHP heats aged for extended times at 700°C, Figure 34. The increase in % IG fracture of the High C and the Medium C heats was proportional to their bulk C contents at a given aging time, thus these results indicate that the amount of grain boundary carbides control low temperature embrittlement.

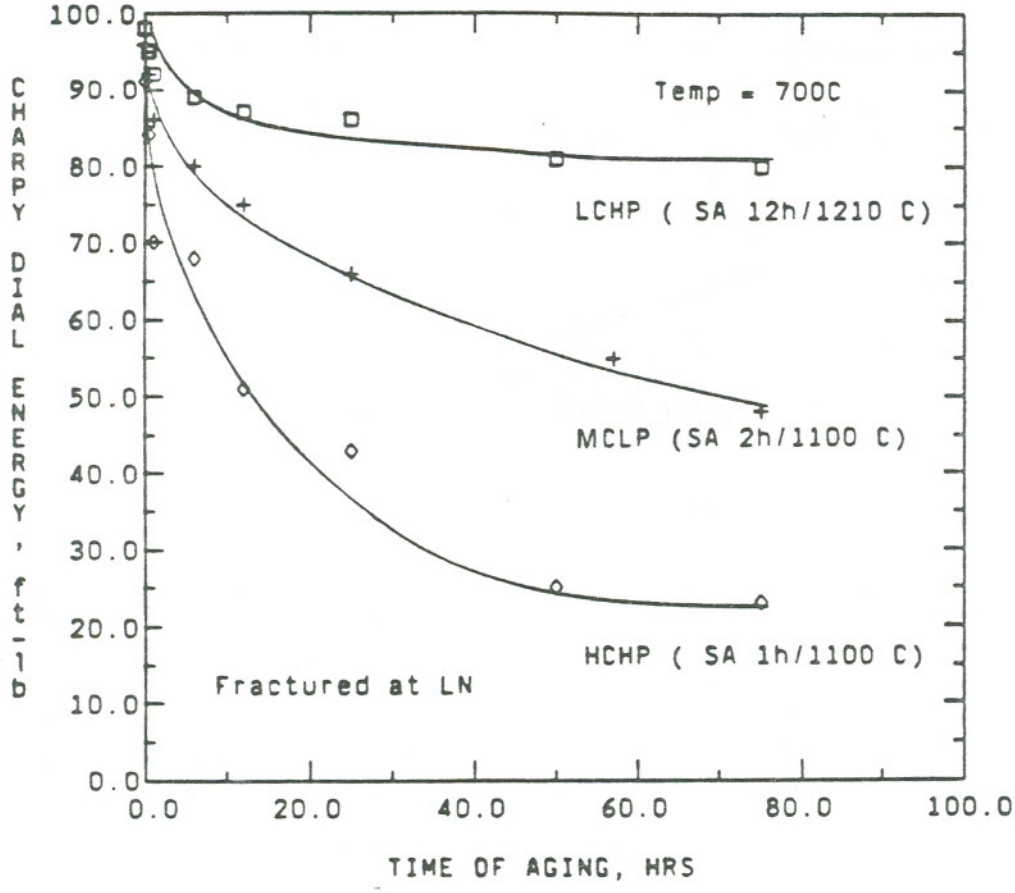

FIGURE 33. Reduction in Impact Energy as a Function of Heat Treatment Time at 700°C for HCHP, MCLP, LCHP 304 SS.

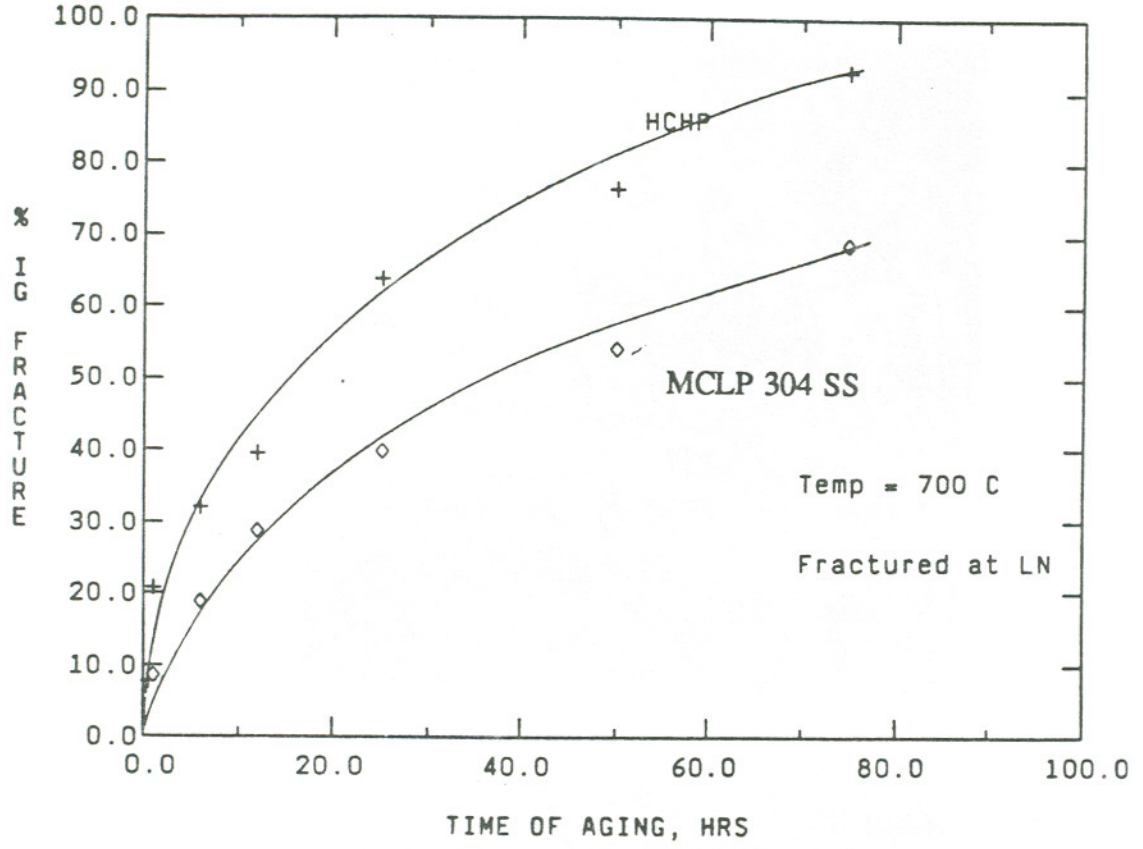

FIGURE 34. Variation of IG Fracture with Aging Time at 700°C.

The reduction of impact energy was found to coincide with a change in the fracture mode from transgranular to IG. The complementary relationship of the impact energy and the % IG fracture is illustrated in Figure 35, for the High C heat. This dramatically illustrates that lower impact energies are associated with IG fracture and higher impact energies with ductile fractures. The SEM micrographs in Figure 36a, b show the development of IG fracture in the High C heat. The % IG fracture ranges from zero for the SA material to nearly 93% for the sample aged 75 hours at 700°C.

FIGURE 35. SEM Micrographs for SA and 75 Hours at 700°C Material Showing Development of IG Fracture at 700°C in MCLP 304 SS.

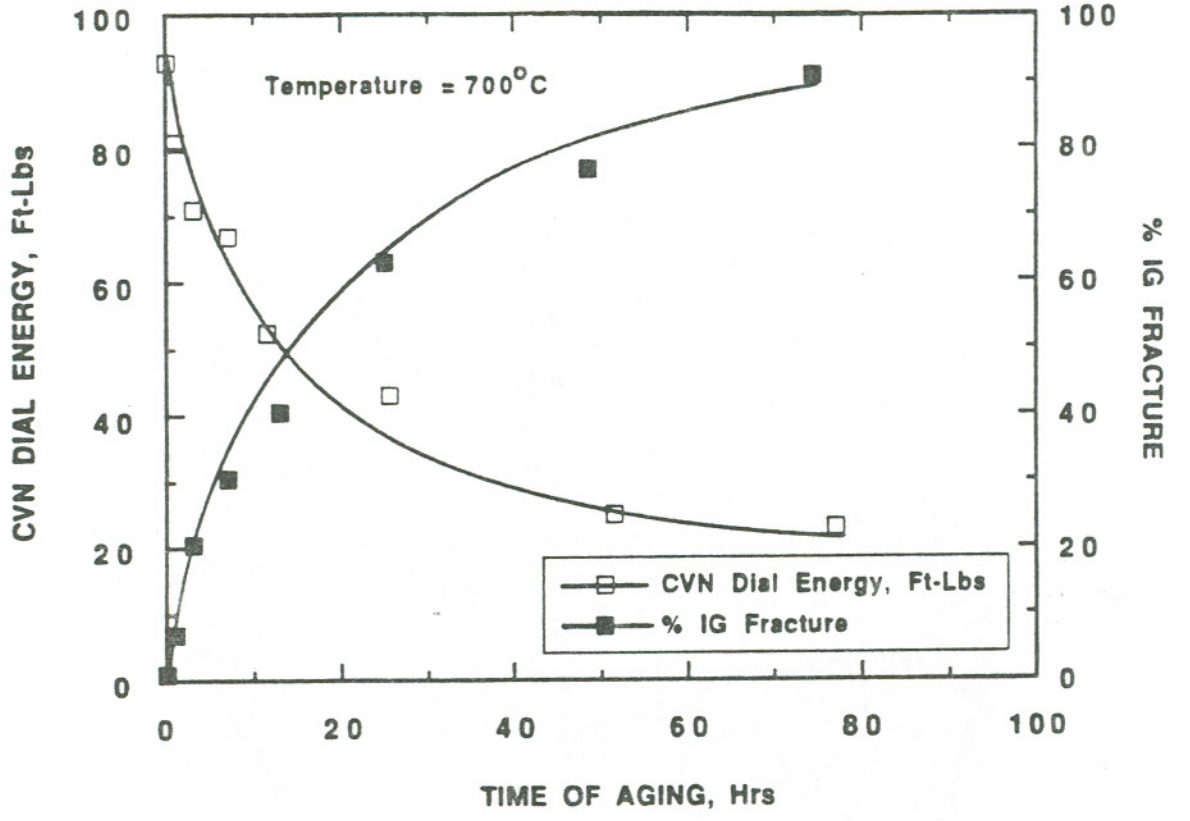

FIGURE 36. Correlation of CVN Impact Energy and IG Fracture as a Function of Aging Time at 700°C for HCHP 304 SS.

The aged specimens were then subjected to the EPR test in order to determine whether carbide growth, as indicated by increasing EPR, continues throughout the aging cycle. The presence of a highly sensitized structure in these heats was established by the EPR test; Figures 37 and 38 show micrographs of the EPR test attack. These test results imply the presence of grain boundary carbide precipitation. The graphs in Figure 39 illustrate the variation of EPR-DOS for the High C and Medium C heats as a function of % IG fracture obtained. The EPR-DOS shows an excellent linear correlation with the % IG fracture. The HCHP heat shows a relatively larger drop in impact energy than the MCLP heat and also shows a higher EPR-DOS

number by virtue of having a higher C content. The EPR results normalize the effect of bulk C content and show both heats following the same trend, Figure 39. It is expected that the carbide precipitation mechanism is the only one under consideration in the MCLP heat. Thus, carbide precipitation at the grain boundaries is postulated to control the IG embrittlement in the above heats.

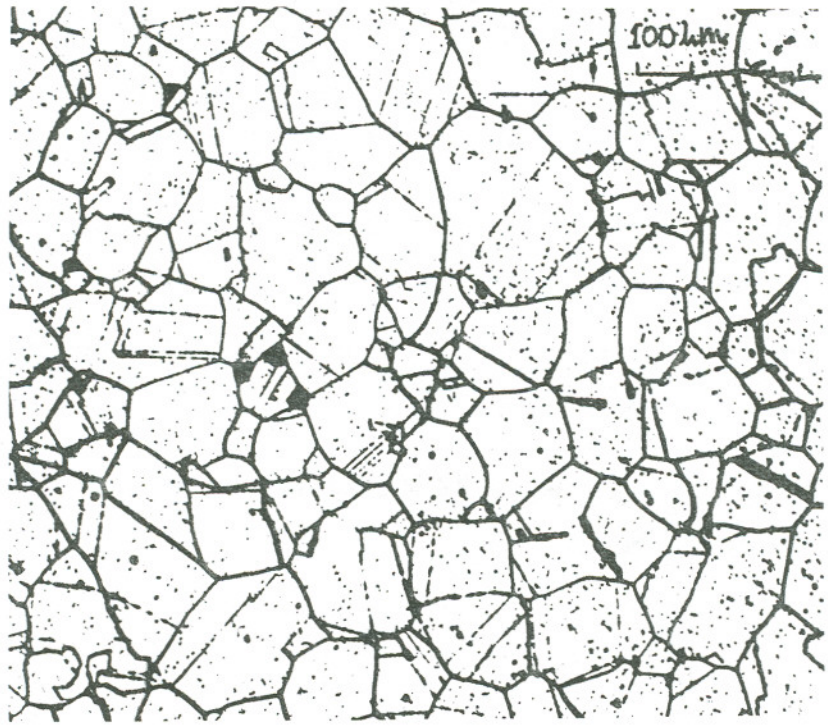

FIGURE 37. Optical Micrograph Illustrating EPR Test Grain Boundary Attack for HCHP 304 SS After Aging at 700°C.

FIGURE 38. Optical Micrograph Illustrating EPR Test Grain Boundary Attack for MCLP 304 SS After Aging at 700°C.

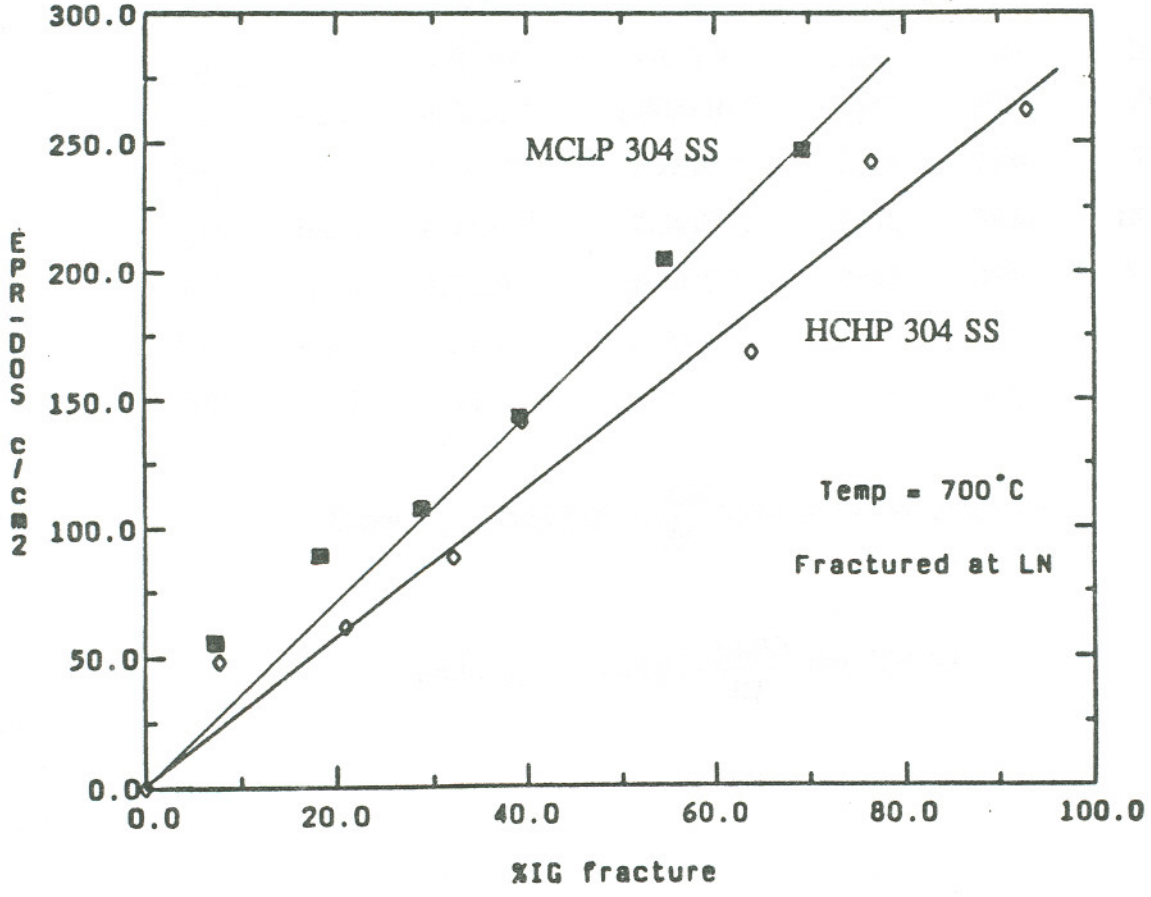

FIGURE 39. Correlation of EPR-DOS and IG Fracture as a Function of Aging Time at 700°C for HCHP and MCLP 304 SS.

A set of experiments directed towards assessing the effect of carbide size and density were also undertaken. This consisted of subjecting the high and medium C heats to aging temperatures ranging from 900 to 700°C. The aging time at each temperature was varied such that the diffusion distances of Cr and p were kept constant for these treatments, see Table 7. Figure 40 shows the variation of impact energy for the HCHP heat for different temperatures. The impact energy decreases with decreasing temperature while EPR-DOS increases rapidly with decreasing temperature. Similar results for the MCLP heat are presented in Figure 41. The increase in impact energy with increasing aging temperature is postulated to be associated with a decrease in carbide density and an increase in carbide size expected to take place with increasing temperature.

TABLE 7. Heat Treatment Schedule at Different Temperatures for 304 Laboratory Heats

Temperature		D_p	D_{Cr}	$\sqrt{D_p t}$	$\sqrt{D_{Cr} t}$	Time
°C	K	cm^2/sec	cm^2/sec	nm	nm	hrs
650	923	4.7×10^{-14}	1.003×10^{-15}	2448	3950	350
700	923	2.2×10^{-13}	5.2×10^{-15}	2448	3950	75
750	1023	8.9×10^{-13}	2.3×10^{-14}	2448	3950	18.66
800	1073	3.1×10^{-12}	8.8×10^{-14}	2448	3950	5.28
850	1123	9.9×10^{-12}	2.99×10^{-13}	2448	3950	2.0
900	1173	2.8×10^{-11}	9.2×10^{-13}	2448	3950	1.0

$$Using\ D_p = 0.51 \exp\left(\frac{-55{,}000}{RT}\right) for\ a\ Fe\text{-}Ni\text{-}P\ ternry$$

$$and\ D_{Cr} = 0.08 \exp\left(\frac{-58{,}000}{RT}\right) for\ 304\ SS$$

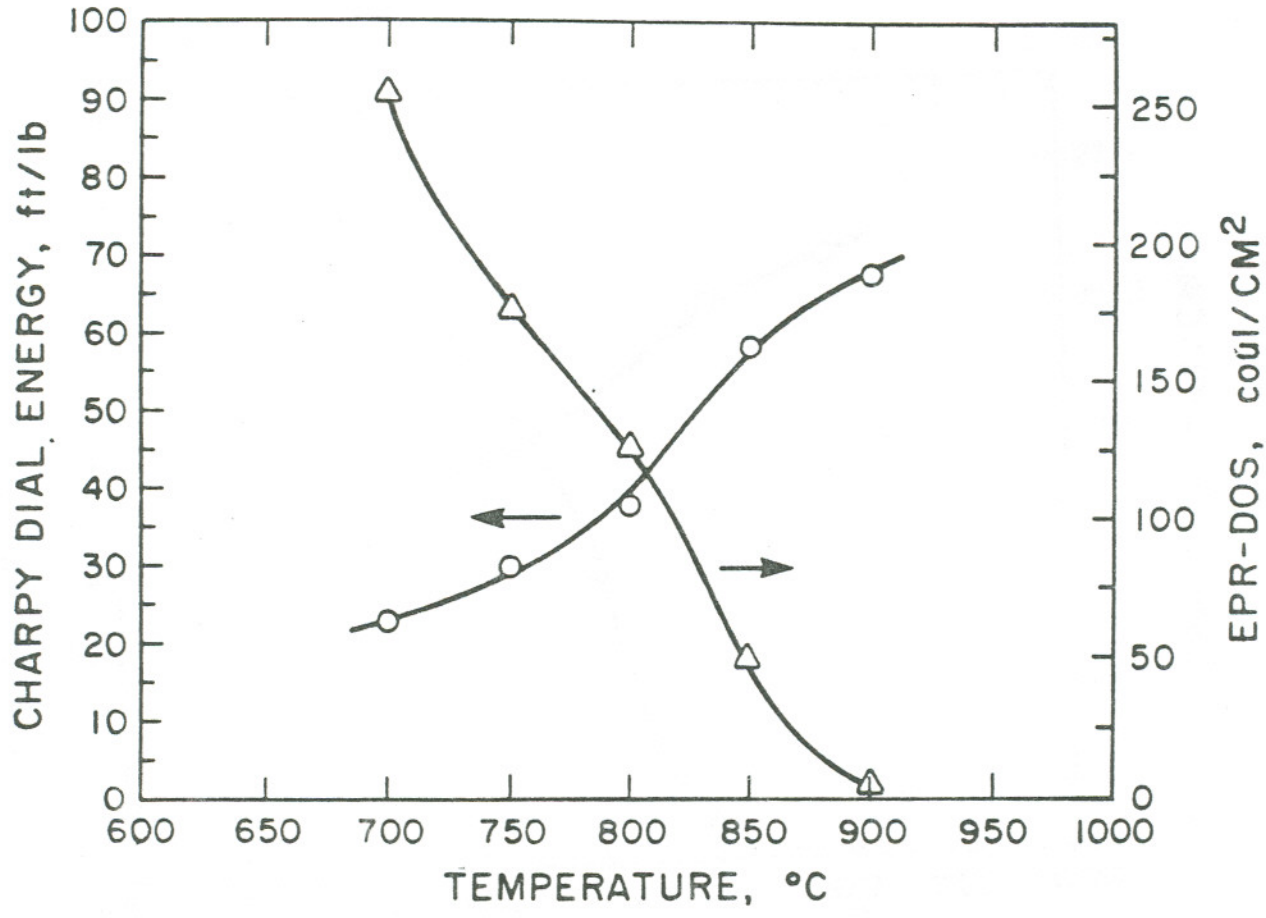

FIGURE 40. Correlation of Reduction in Impact Energy and Increase in EPR-DOS at Constant Chromium Diffusion Distance Aging Times for HCHP 304 SS as a Function of Heat Treatment Temperature.

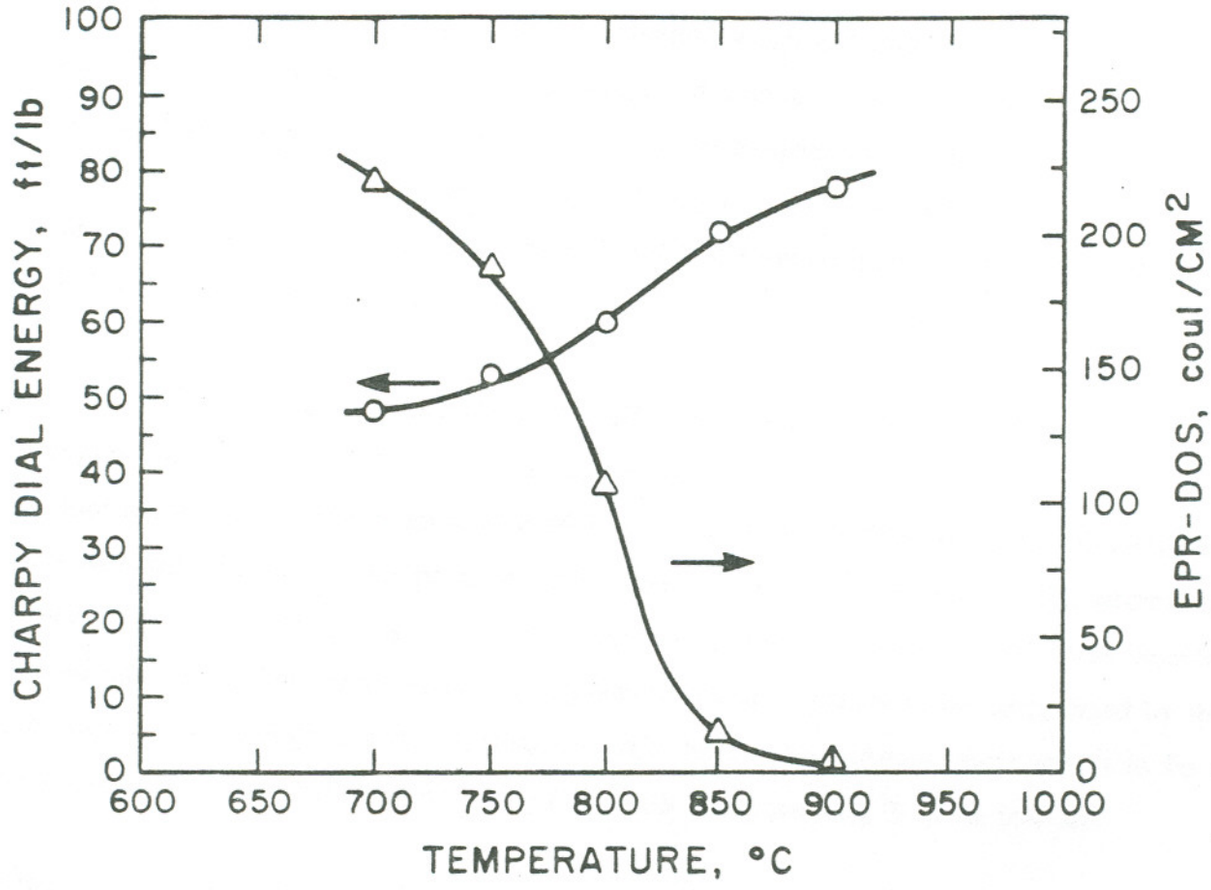

FIGURE 41. Reduction in Impact Energy and Increase in EPR-DOS for MCLP 304 SS as a Function of Heat Treatment Temperature at Constant Chromium Diffusion Distance Aging Times.

The decrease in EPR with increasing aging temperature is a more complex phenomenon, as the measured value is a function of Cr depletion width and minimum, both of which are expected to change as a function of temperature and time at temperature; an illustration of the expected change in Cr minimum as a function of test temperature is illustrated in Figure 21.[35] The EPR-DOS for the HCHP heat (0.061 wt% C) is consistently higher, at a given aging temperature, than that for the MCLP heat (0.043%C) showing that C pushes the stability of carbides to higher temperatures.

The fracture morphologies for the HCHP heat aged at different temperatures are shown in Figure 42. The amount of IG fracture decreases with increase in aging temperature. The fracture morphologies vary from around 16% at 900°C to nearly 50% at 750°C. Growth rate increases with increasing temperature while ease of nucleation increases with decreasing temperature; this leads to large well-spaced carbides at high temperatures and small closely-spaced carbides at low temperatures. Intergranular fracture appears to be accentuated by the presence of small, high density carbides on grain boundaries. Again, there seems to be a reasonable correlation between increasing EPR-DOS and increasing % of IG fracture.

Effect of Grain Boundary Martensite

This section discusses the potential for formation of athermal martensite at the Cr depleted regions adjacent to the grain boundaries, and martensite's anticipated effect on the IG embrittlement susceptibility under impact loading conditions in 304 SS. Athermal martensite formation along sensitized grain boundaries has been previously reported and found to severely affected impact toughness.[14] It is hypothesized to be a function of the local Cr content, favorable crystallographic orientation and strain inhomogeneities.

Figure 43 demonstrates that there is a considerable difference in the decrease in the impact energy between ambient and LN of programmatic specimens indicating a potential

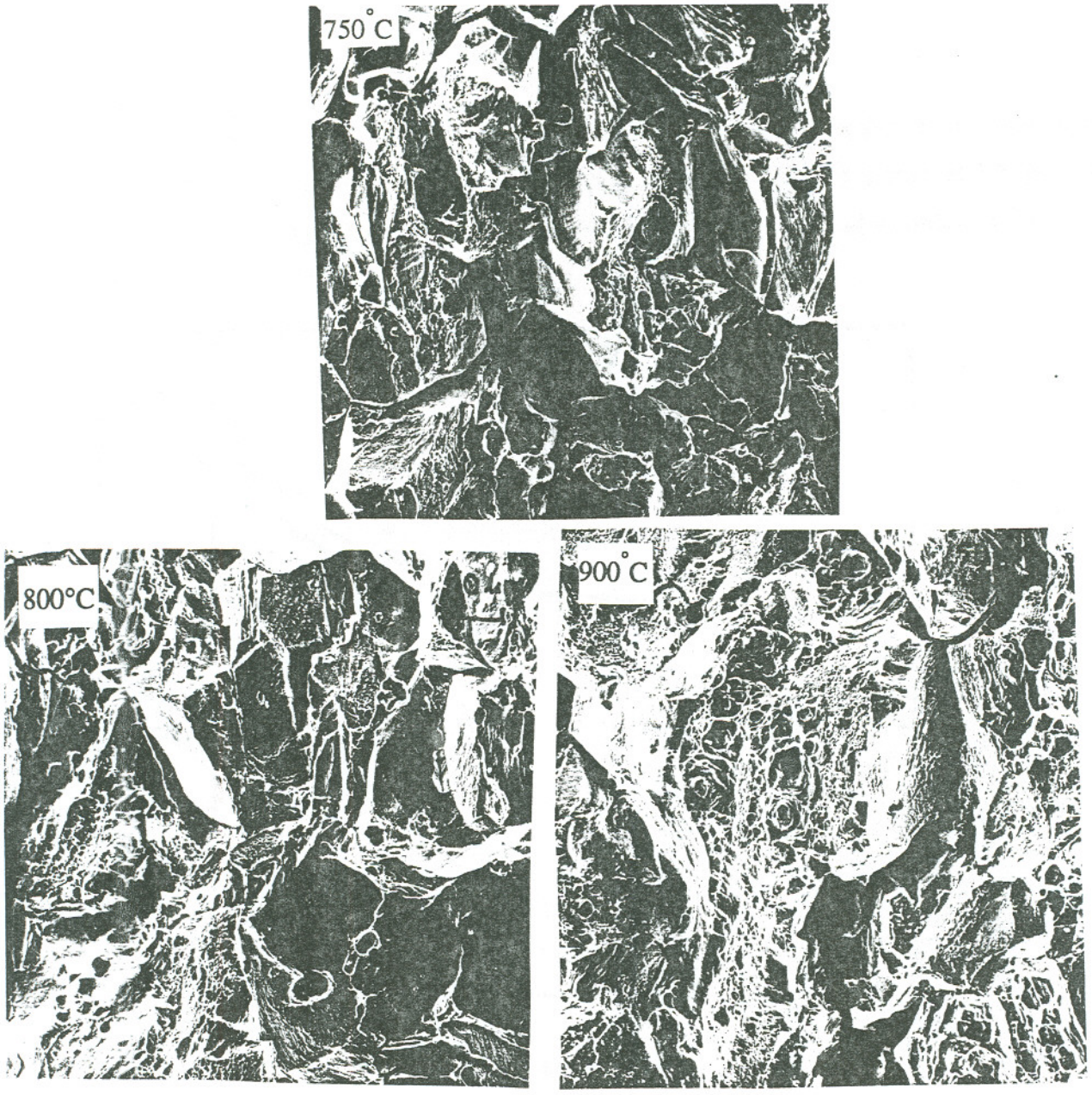

FIGURE 42. SEM Micrographs of Fracture Morphologies of HCHP Heat Aged at Different Temperatures.

for α' induced material embrittlement. The test used to determine whether or not martensite affected LN impact values for these alloys was to subject specimens to a soak at LN prior to room temperature testing. This low temperature soak would be expected to induce α' at grain boundaries and thus embrittle room temperature specimens.

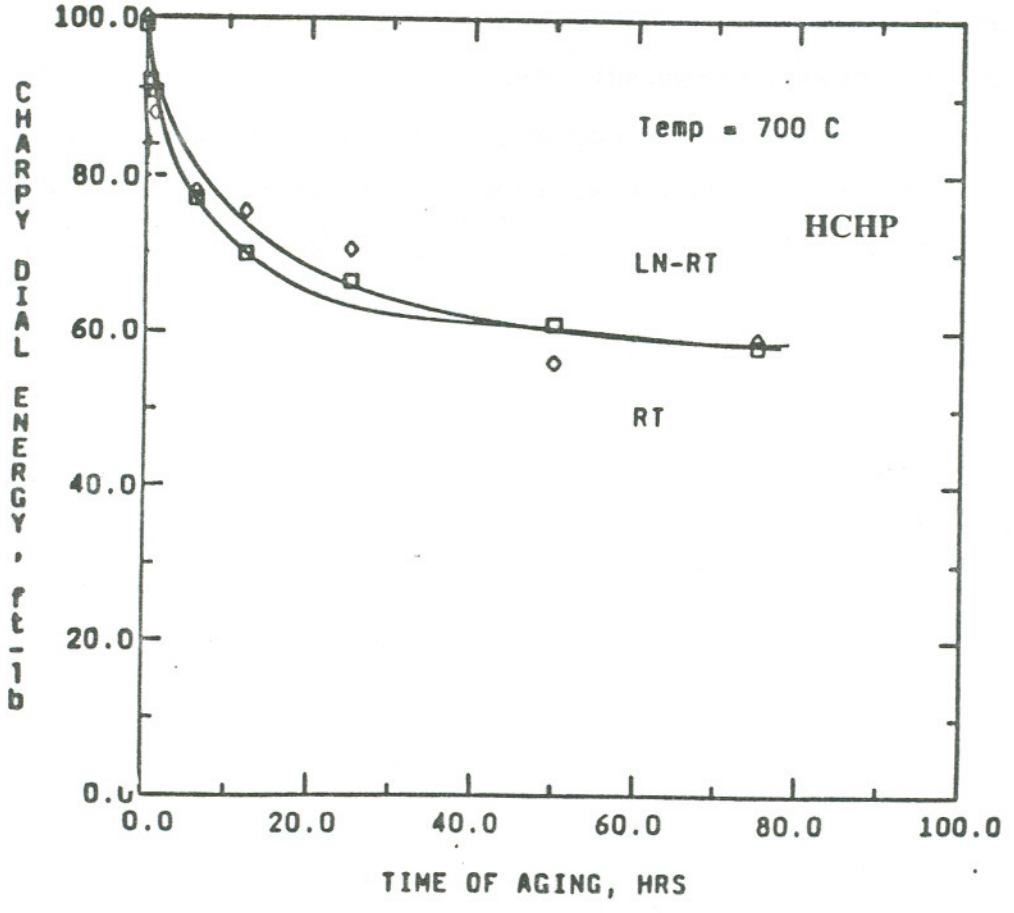

FIGURE 43. Low Temperature Exposure Effects on Embrittlement due to Aging at 750°C for HCHP 304 SS Indicating Absence of Grain Boundary Martensite.

However, no differences in impact energies between the room temperature specimens with and without quenching to LN temperature was found, Figure 43. Thus it is concluded that athermal martensite formation at Cr-depleted grain boundaries did not occur in these steels on cooling to LN, similar to the findings for 316 SS. Thus, grain boundary martensite formation is not necessary to cause significant embrittlement in Type 304 SS.

Bulk compositional correlations with martensite do suggest that martensite could potentially form between room and LN temperature in highly Cr-depleted grain boundary regions. According to the formula for the M_s temperature given by Eichelman and Hull $M_s(°C) = 1302 - 42\ (\%C_r) - 61\ (\%Ni) - 33\ (\%Mn) - 28\ (\%Si) - 1667\ (\%[C+N])$ the M_s temperatures vary from well below LN temperatures to above room temperature as a function of Cr content, Figure 44. It is evident that, for bulk chemistry of the laboratory heats, the formation of athermal martensite above room temperature is extremely unlikely. The question is whether α' selectively forms in a very thin region around grain boundaries exhibiting chromium depletion. The LN soak - room temperature test results indicate no α' formation even though alloys with bulk concentrations similar to those found in the Cr depleted regions would be expected to exhibit LN induced α'.

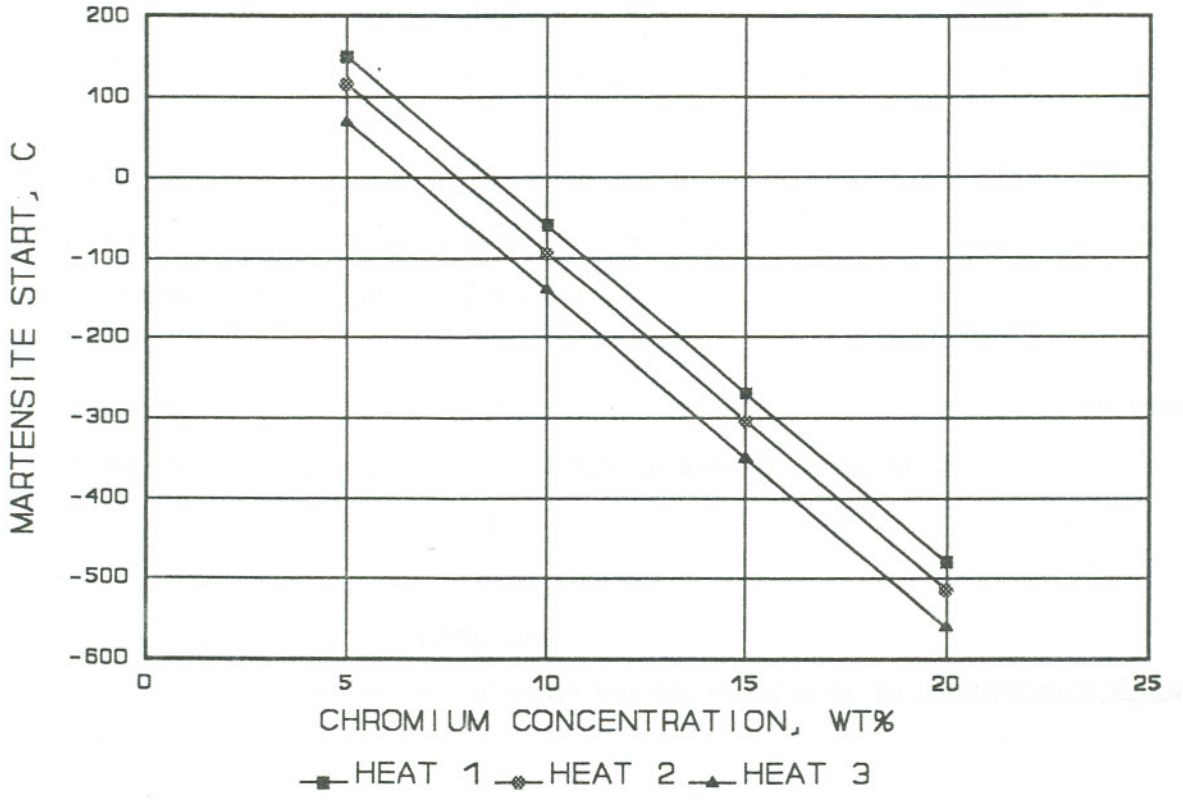

FIGURE 44. Prediction of M_s for 304 SS Heats as a Function of Cr Concentration.

INTERACTION EFFECTS AND RANKING SYSTEM

This section gives an overview of the results obtained for the 304 SS and provides a 'ranking system' of the various embrittlement mechanisms for the laboratory heats under consideration. The IG embrittlement obtained was found to closely relate to carbide precipitation. Sigma phase, when present, acts as a potent embrittling agent. The amount and distribution of sigma phase is a function of the amount of delta-ferrite in the heats and the heat treatment and can induce either IG or transgranular embrittlement. Phosphorus segregated values of up to 8 to 18% were not found to promote IG fracture. Again, as in 316 SS, specimens with a high density of IG carbides with and without P segregation were embrittled. Grain boundary athermal martensite formation was not observed in these heats.

Thus, in conclusion, for the 304 laboratory heats under study, the ranking of the various embrittlement mechanisms in the order of decreasing potency appear to be:

- Sigma phase precipitation
- Grain boundary carbide precipitation
- Grain boundary P segregation

Grain boundary athermal martensite formation was not found to be an embrittlement factor in these alloys.

Comparison of 304 and 316 SS Results

This section discusses the similarities and differences of embrittlement results observed between the 316 and 304 type of SSs.

- Essentially, carbide precipitation was found to be the dominating IG embrittlement mechanism in both these alloys. It produces nearly 90% IG fracture under high strain rate conditions.

- Auger data indicated the 304 SS alloy exhibited twice as much grain boundary precipitation as the 316 SS; a factor of four was expected.

- Grain boundary athermal martensite formation was not observed in either of alloys

types.

- Sigma formation from retained delta ferrite was observed in the LCHP heat of 304 SS and proved to be a serious embrittlement factor in 304 SS. Sigma phase precipitation from retained delta ferrite can also occur in Type 316 SS, depending on the chemistry and if subsequent thermomechanical processing is such that it allows for the presence of delta-ferrite. Embrittlement by sigma is expected to be similar for both alloy Type if either alloy contain delta-ferrite prior to aging treatment. Sigma formation from the austenite phase is possible, however, it occurs at very long aging times.

CONCLUSIONS

The causes for embrittlement in Type 304 and 316 austenitic SSs have been investigated. The potential causes for high strain rate induced embrittlement have been classified as

- Grain boundary carbide precipitation
- Grain boundary P segregation
- Grain boundary martensite formation
- Sigma phase precipitation

The primary conclusions and observations resulting from the current work are listed below:

- The impact energy of heats containing a substantial amount of C decreases rapidly as a result of heat treatment in the sensitization range. Temperatures below or above this critical temperature range result in very little embrittlement.
- Intergranular embrittlement can be produced solely by grain boundary carbide precipitation.
- Phosphorus played only a secondary role, if any, in the development of IG fracture. Whether this is due to the inability of P to promote decohesion of grain boundaries or the low levels of segregation seen is not clear.
- No formation of grain boundary athermal martensite was observed for the bulk compositions such as present in these heats. Its presence at the grain boundaries is not required to cause a massive drop in impact toughness.
- The distribution and morphology of grain boundary carbide precipitates significantly affects the impact toughness of the steels. Carbides formed at high aging temperatures are coarser and the impact drop is not as pronounced as caused by those formed at lower temperatures where the carbides formed are fine and dense.
- Precipitation of sigma from retained delta-ferrite takes place at very short aging

times and severely degrade the impact toughness. The precipitates can occur on both IG and transgranular sites depending on the SA treatment.

- A maximum of 10% P for 316 SS and 20% P for 304 SS, assuming monolayer coverage was observed at the grain boundaries. This amount was not enough to cause embrittlement in these steels. However, it is possible that a higher amount may well induce an embrittling effect.

REFERENCES

1. Weiss, B. and Stickler, R., Metallurigal Transactions, vol. 3, p. 851, April 1972

2. Danyluk, S., Wolke, I., Metallurgical Transactions, vol. 17A, pp. 663-668, April 1986.

3. Stoter, L.P., Journal of Materials Science, vol. 16 pp. 1039-1051, 1981.

4. Hoke, J.F., Wylie, R.D., Proc. ASTM, vol. 57, p. 821, 1967.

5. Tseng, T.D., Gan, D., and Kao, P., Material Science and Engineering, vol. 95, pp. 73-80, 1987.

6. Chen, S.Y. and Gan, D., Material Science and Engineering, vol. 84, pp. 65-76, 1989.

7. Danyluk, S. and Park, Jong-Yul, Scripta Metallurigica, vol. 16, pp. 769-774, 1982.

8. Gordon, G.M., "Stress Corrosion Cracking and Hydrogen Embirttlement of Iron Base Alloys", National Association of Corrosion Engineers, Houston, Texas, p., 843, 1973.

9. Atteridge, D. G., Bagchi, A., Bruemmer, S. M., and Charlot, L. A., Influence of Grain Boundary Carbides and Phosphorus Segregation on the Low-Temperature Intergranular Embrittlement of Type 316 Stainless Steel, Scripta Metallurgica, vol. 23, No. 9, pp 1549-1554, Pergamon Press, 1989.

10. Bruemmer, S. M., "Grain Boundary Chemistry and Intergranular Failure of Austenitic Stainless Steels," Materials Science Forum, vol. 46, pp. 309-334, 1989.

11. Danyluk, S. and Poole, J.Y., Scripta Metallurgica, vol. 16, p., 769, 1982.

12. Losch, W.H.P., Scripta Metallurgica, vol. 11, p-., 889-994, 1977.

13. Briant, C.L. and Banerji, S.K., International Metallurgical Review, vol. 23, p., 164, 1978.

14. Gan, D., Metallurgical Transactions, vol. 13A, p. 2155, 1982.

15. Briant, C.L., and Andresen, P.L., Metallurgical Transactions, vol. 19A, pp. 495-504, Mar 1988.

16. Mulfor, R.A., McMahon, C.J., Pope, W.P., and Geng, G.C., Metallurgical Transactions, vol. 7A, p., 1183, 1976.

17. Senior, B.A., Havel, R., and Neale, B.K., Materials Science and Technology, vol. 5, pp.

1090-1094, November 1989.

18. Briant, C.L., "On the Chemistry of Grain Boundary Segregation and Grain Boundary Fracture", General Electric Company Report, 1988.

19. Guttman, M., Surface Science, vol. 53, pp. 213-227, 1975.

20. McLean, Grain Boundaries in Metals, Clarendon Press, Oxford, 1957.

21. Hondros, E.D., Seah, M.P., Scripta Metallurgica, p. 1007, 1972.

22. Briant, C.L., Acta Metallurgica, 1988.

23. Gruzin, P.L. And Mural, V.V., Fiz. Metal, M17, p. 62.

24. Guttmann, M. and Dumoulin, Ph., "Tan-Tai, N.", Corrosion-NACE, vol. 37, no. 7, July 1981.

25. Briant, C.L., Metallurgical Transactions, vol. 18A, pp. 691-699, April 1987.

26. Briant, C.L., and Andresen, P.L., Metallurgical Transactions, vol. 19A, pp. 495-504, March 1988.

27. Hanninen, H., and Minni E.: Metall. Trans., 1982, 13A, 2281.

28. Lumsden, J.B. and Stocker, P.J., Scripta Metallurgica, vol. 15, pp. 1275-1298, 1981.

29. Suzuki, S., Hanada, R., and Kumura, H., Material Science and Engineering, vol. 80, pp. 75-85, 1986.

30. Hondros, E.H. and McLean, D., Phil. Mag., vol. 29, p. 771, 1974.

31. Seah, M.P., Proc. Roy. Soc., vol. 349A, p. 535, 1974.

32. Bernstein, I.M. and Rath, B.B., Metallurgical Transactions, vol. 4, p. 1545, 1973.

33. Natesan, K. and Kassner, T.F., Nucl. Technol., vol. 19, No. 46, 1973.

34. Deighton, M., "Solubility of $M_{23}C_6$ in Type 316 Stainless Steel," J. Iron Steel Inst, p. 1012, November 1970.

35 Bruemmer, S. M., "Quantitative Measurement and Modelling of Sensitization Development in Stainless steels", DOE-NE-37963-7 Oregon Graduate Institute (OGI), Beaverton, November 1988.

36. Lai, J.K.L., Material Science and Engineering, vol. 61, p. 101, 1983.

37. Stawstrom, C. and Hillert, M., J. Iron Steel Inst, p. 77, January 1969.

38. Tedmon, C.S., Jr., Vermilyea, D.A., and Rosolowski, J.H., J. Electrocham Soc, vol. 118 no. 2, p. 192, 1971.

39. Hall, E.L. and Briant, C.L., Metallurgical Transactions, vol. 15A p. 793, May 1984.

40. Fullman, R.L., Acta Metall., vol. 30, p. 1407, 1982.

41. Chang, L. and Gan, D., Material Science and Engineering, vol. 95, pp. 125-136, 1987.

42. 262, ASTM Book of STandards, A, 16, p. 1, ASTM, Philadelphia, Pennsylvania, 1978.

43. Bruemmer, S.M., Corrosion, vol. no. 1, p. 27, January 1986.

44. Clarke, W.L., "The EPR Method for the Detection of Sensitization in Stainless Steels", NUREG F-0252-1, U.S. Nuclear Regulatory Commission, 1976.

45. Lee, J.B., Corrosion, vol. 42, no. 2, p. 106, February 1986.

46. Bain, R. H., Aborn, Trans, Amer. Soc. Steel Treat., vol. 18, p.837. 1930.

47. Eichelman, G.H., and Hull, F.C., Trans. ASM, vol. 45, p. 77, 1953.

48. Hall, E.O., and Algie, S.H., Met. Rev. vol. 11, p. 61, 1966.

49. "Handbook of Stainless Steels", Mcgraw-Hill Book Company, pp. 4-61, 1977.

50. Senior, B.A., Material Science and Engineering, vol. 100, p. 219, 1988.

51. Holt, R.M., and Nicholson, O.P., J. Iron Steel Inst., vol. 200, p. 715, 1962.

52. Newell, H.D., Met. Prog. pp. 977-1028, 1946.

53. Standards, ASTM Book of E-112-85, 16, p. 1, ASTM, Philadelphia, Pennsylvania, 1978.

54. Standards, ASTM Book of E-23-86, 16, ASTM, Philadelphia, Pennsylvania, 1978.

55. U.S. Nuclear Regulatory Commission, NRC-G-04-87-105, Semi Annual Report, June 1988.

56. White, W.E. and Le May, I., Metallography, vol. 3, pp. 35-50, 1970.

57. Weiss, B., and R. Stickler: Metall. Trans., vol. 3, p. 851, 1972.

58. Schaeffler, A. L.: Met. Prog., vol. 56, p.680, November, 1969.

59. Briant, C.L., Acta Metall, vol. 31 no. 2, pp. 257-266, 1983.

VITA

The author was born on April 1, 1966 in the southern city of Bangalore, India. He moved to Bombay when he was a year old. The author had all of his education in Bombay. He graduated with a B.Tech degree in Metallurgical Engineering from I.I.T. Bombay in June 1987. Upon graduation, he worked for a year at M.N.Dastur Consulting Engineers(P) Ltd. in their computer division.

The author then joined the Oregon Graduate Institute for a M.S. degree in Materials Science and Engineering in Sept 1988. He is currently pursuing his Ph.D degree in Materials Science and Engineering at the University of Texas at Austin.

List of publications include:

(1) "Deformation effects on intragranular carbide precipitation and transgranular chromium depletion in type 316 stainless steels"; Corrosion, vol 47, no. 12, p 939-947, Dec. 1991.

(2) "Mechanisms of deformation induced grain boundary chromium depletion(sensitization) development in type 316 stainless steels", Metallurgical Transactions, vol 22A, p 2917-2934, Dec. 1991.